

# Mutual information of a fully connected neural network learning process

Natalia Copete, Diego A. Garzon, J.M. Pedraza and J. Forero-Romero\*

(Dated: June 29, 2019)

Artificial Neural Networks (ANN) were developed in the last 50 years with the intention to mimic the brain's process to handle stimuli. Thanks to increasing computing power at lower costs, ANN have finally become a central feature to the success of the broader Machine Learning (ML) community. Biological studies have found that weak correlations among pairs of neurons coexist with strong correlations in the states of population as a whole. In this work we want to test whether these correlations also hold for ANN. To this end we train fully connected neural network (FCNN) for different classification tasks and measure the mutual information (MI) between groups of neurons at different stages of the learning process of the mentioned neural network. Our results suggest that FCNNs behave as their biological counterpart, that is, the global MI is larger than the local one by an order of magnitude. We finalize by discussing the implications of these results for ANN training.

## I. INTRODUCTION

Artificial neural networks (ANN) are a computational model that was created with the aim of mimicking the brain's process to handle stimuli [1]. Thanks to the revamping changes in computer power that accompanied the end of the 20th century, ANN became one of the most important algorithms in the machine learning (ML) community, showing a remarkable performance in an high variety of classification and recognition tasks such as chemical reactivity [2], diagnostic prediction of cancers [3] and language processing [4], among others.

A standard ANN consists of a sequence of layers of processors (neurons) that produce a succession (in time) of real-valued activations (Fig 1). The activation of a neuron of a particular layer, is a non-linear function of the activation of the neurons of the previous layer; and also, it is a function of the connections between that particular neuron that is being activated and the neurons of the previous layer. Those connections, are called weights and they can be assimilated as the axons of the ANN. Partly, the learning process of an ANN consists on the optimization of all the weights present in the network [5]. When all the neurons from a particular layer are connected to all the neurons of the previous layer, for all the layers in the network, it is possible to talk about a fully connected network (FCNN).

Despite their great success, ANN are often treated as "black boxes" i.e. the way that information is processed inside the ANN is not well understood [7]. Recent attempts to solve that problem, have used the perspective of information theory (IT). In particular, the notion of mutual information has been presented as a useful approach to understand ANN [7, 8]. In IT, mutual information (MI) is a measure of the degree of correlation of two random variables; that is, how much (information)

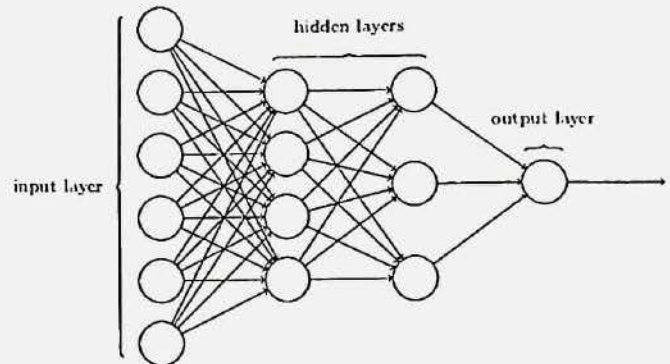


FIG. 1. Basic structure of an artificial neural network[6]

we can know about one variable, by knowing the other [9, 10]. Formally, the MI  $I(X, Y)$  of two random variables X and Y is defined as

$$I(X, Y) = \sum_{i=1}^{m_x} \sum_{j=1}^{m_y} p(x_i, y_j) \log \frac{p(x_i, y_j)}{p(x_i)p(y_j)}, \quad (1)$$

where  $x_i$  and  $y_j$  are particular outcomes of the random variables X and Y respectively and  $m_x$  and  $m_y$  are the number of possible outcomes of the random variables X and Y respectively[10]. Depending on the base of the logarithm, the units of MI vary [11]. In the case of having many random variables N we can define the multivariate MI as [12]

$$I(X_1, \dots, X_N) = \sum_{i=1}^{m_x} \dots \sum_{j=1}^{m_N} p(x_1, \dots, x_N) \log \frac{p(x_1, \dots, x_N)}{p(x_1) \dots p(x_N)}. \quad (2)$$

At this point, it is important to mention that, even if MI has been already considered for analyzing ANN, there is no unique way in which this notion might be used. In the present work, we aimed to use it as a tool to compare the behaviour of biological neural networks and that of ANN. More precisely, our purpose was to evaluate if the observation reported by Schneidman and co-workers[13] hold true for ANN, that is, we wanted to

\* n.copete@uniandes.edu.co; da.garzon1@uniandes.edu.co; Also at Universidad de los Andes, Bogota, Colombia.

test if weak correlations among pairs of neurons coexist with strong correlations in the states of population as a whole[13]. Such a behaviour makes sense from the biological point of view since the information owned by, for example, an eye cell, hardly allows us to know what information is in another eye cell. But, it is easy to see that the information owned by a sufficiently big group of eye cells can be enough to know about the information in the rest of the cells of the network and would allow us to know the image that is being seen by the eye as a whole. From the biological point of view, it is important to mention that the results reported by Schneidman and co-workers were obtained from the analysis of retina cells from larva tiger salamander. Additionally they reported a similar behaviour in networks of cultured cortical neurons.

We start by introducing the experimental details related to the data set, the neural architecture and the MI measurement. Then, are presented the obtained results through a set of graphs that relate different magnitudes of interest such as accuracy, training time and MI. We finalize by discussing about the similarity with the biological case that we found and the possible implications of our results, as well as the prospects of our work.

## II. EXPERIMENTAL DETAILS

All the study was made in Python 3.5.2 with original code using the NumPy, Matplotlib and TensorFlow packages for graphing, data analysis and neural network building and training.

### A. Data set

**MNIST.** - The MNIST data set were used for training the neural networks. [14] This data set consists in handwritten numbers from 0 to 9 with a training and test set with 60 000 and 10 000 samples, respectively. The samples are 28x28 pixels 8-bit gray-scale images and were normalized to the dynamic range [0, 1] as well as flattened.

### B. Neural network architecture

The neural network consists of two fully connected layers, one hidden and the output layer. The first one with a variable number of neurons from 3 to 16. Each neuron with a weight and a bias optimized within the learning process and a sigmoid function as a non-linear activation function. The second layer consist of a single neuron with a *softmax* function, which it's able to estimate a probability for each label to correspond to the sample.

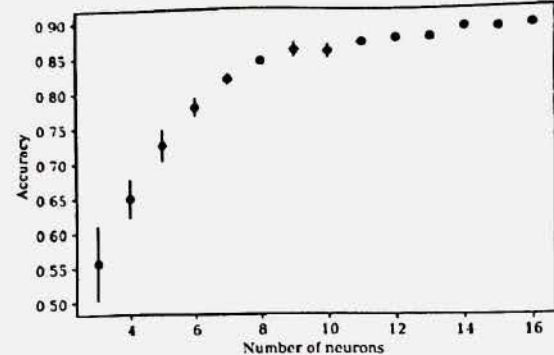


FIG. 2. The accuracy of the trained neural networks on the test set with respect to the number of neurons.

### C. Learning process

Each architecture (i. e. the number of neurons in the first layer) was trained three times with a randomized data set of one unique batch with 500 epochs. The training process was done using a cross-entropy function as loss function and an Adam optimizer with a learning rate of  $10^{-3}$ .[15] In each epoch, we measured the accuracy of the network with the test set as well as the mutual information between the neurons in the layer.

### D. Mutual information measurement

Two different MI were measured in its normalized version, with a normalization constant equal to  $(n - 1)^{-1}$ , where  $n$  is equal to the number of neurons.[12] For the measurement of the normalized mutual information (NMI) we established two states for each neuron, activated or deactivated and in order to decide we set a threshold equal to 0.5, due long as we tested different values for this threshold and found a similar behavior for the NMI. We calculated the NMI for pairs of neurons, with only four possible combinations and for all the neurons in the layer with  $2^n$  possible combinations. The probability of each state was found establishing the repeating of each event in the output of the first layer corresponding to every sample in the training data, later it was divided for the number of samples (i. e. 60 000) to obtain a probability.

## III. RESULTS

### A. Training process

We trained 14 different networks. Through this process, as was expected, we see an increase in accuracy proportional to the number of neurons, due it has been seen

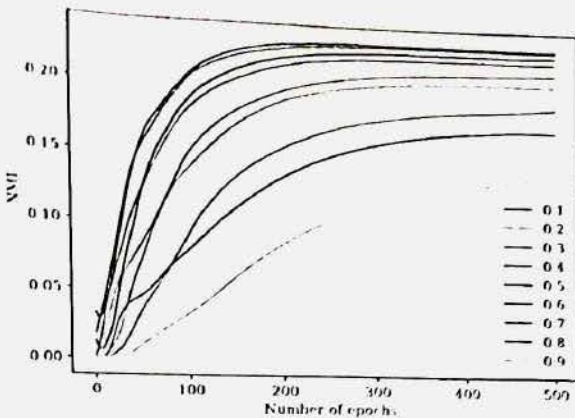


**FIG. 3.** Normalized Mutual Information (NMI) through the training process for different thresholds for a hidden layer with 8 neurons.

that more complex architecture means better results in identification problems in ML [5]. However, the increase in accuracy was not linearly proportional to the increasing number of neurons — in some cases, the change in accuracy was so minimal that we cannot attribute any significance to the change in neural population, as can be seen in FIG. 2. Additionally, we see a monotonically descending loss function and, as was expected, the more complex the network, the lower the final value of the loss function.

### B. Measurement of the NMI

In order to measure this quantity we simplify the output of the hidden layer to a binary problem, so each neuron could be either activated or deactivated. Additionally, those states must be controlled by an arbitrary threshold. However, we studied the behaviour of the mutual information altering the value of the threshold. In every case, we observed a monotonically increasing global NMI function, with a large increase in the earlier epochs, as can be seen in the FIG. 3. With this in mind, we decided to establish a 0.5 threshold for the binary problem of activation for each neuron.

### C. Local vs global NMI

We studied the behaviour of the pairwise (local) and the global NMI trough the training of the neural network (Fig.4). In the obtained NMI functions, it is possible to observe the presence of two phases, a fast one in the earlier epochs followed by a slow one. This can be comparable with Shwartz-Zi et al.'s findings [7]. In most cases, we observed globally increasing NMI functions.

Some local NMI functions, however, do not behave monotonically. For instance, some of them have maxima and random changes in their curvature, although the local NMI functions tend to decrease.

Furthermore, we observe an increasing average distance between the final global and local NMI proportional to the growing neural population. In FIG.4, it is possible to notice that, the trained ANN is showing a behaviour comparable to the one presented by Scheidman et al. on the biological case [13]. In fact, for 3 neurons in the single hidden layer, the global and the local NMI present similar values throughout the training process. But, for 8 and 16 neurons, there is a considerable difference between the red line and the black dashed line; such a difference being more evident in the case of 16 neurons. To summarize, it appears that as the performance of the ANN increases, the average distance between global and local NMI also grows.

On the other hand, is interesting to note that in some particular cases the local is bigger than global NMI for a period of time in the training process. This strange behaviour does not make sense in the biological case, due two nearby neurons cannot share a huge amount of information. In other words, if the local is bigger than or similar to the global NMI, some neuron has to contain redundant information. Moreover, this neuron could not be contribute significantly to the identification of the image.

### D. Redundant information in neurons

If we analyze the biological case, the evolution is an optimization process about how to obtain enough information to survive, but spending the less possible energy in the obtaining process. With that in mind, two neurons that get a high mutual information, are coding the same information but wasting two times the energy, so since an ideal perspective the MI between closer neurons must be very low. Applying this concept to the ANNs, an unusual high NMI could means that some neurons are coding the same information, in other words, some neurons are obtaining the same features for the input to get enough information to predict the output.

However, two neurons obtaining the same information is a waste of energy, in the biological case. For that reason, following the biological trend, we propose that this high NMI could show qualitatively, for now, the presence of a redundant neuron, in other words, that the neural network could obtain a good performance without this neuron. Additionally, in the cases that we observed an unusual high local NMI we observed a similar or equal accuracy as well. For instance, the ANN with 16 neurons has a high a local NMI, as shown in FIG.5, and also has

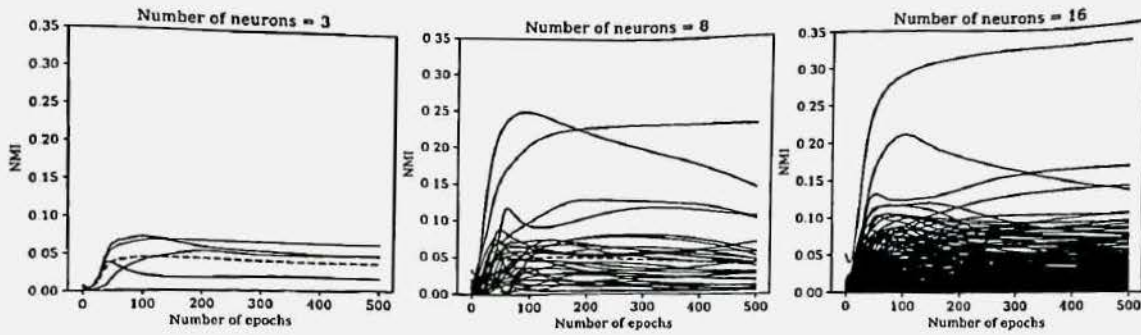


FIG. 4. Comparing the global and local Normalized Mutual Information (NMI) for different numbers of neurons. In red is the global NMI, blue for the locals NMI, and the dashed-black line correspond to the average of the local NMI.

a local NMI function with a large maximum, as shown in FIG. 4. With that in mind, it seems that a neuron is not useful for the codification process and the accuracy obtained for the ANN with 16 and 15 neurons are statically the same.

#### IV. DISCUSSION

We have analyzed the behaviour of a FCCN with one hidden layer through the lens of the information theory showing its similarity with some biological observations in which there is a coexistence between high global MI and low local MI for sufficiently populated neural networks. To do so, as we varied the number of neurons in the single hidden layer, we evaluated two types of NMI during the learning process, a local one (pairwise) and a global one (between all the neurons in the layer).

Additionally, our results suggest the existence of a relation between local NMI and the redundancy of neurons

in the layer. Being able to spot a redundant neuron by measuring NMI could have important implications in the field of ANN. It could allow us to spare computational effort without affecting the performance of the algorithm.

Finally, is worth mentioning the prospects for this work. As the presented results were evaluated considering just one data set and using just one type of activation function, it is in our interests to evaluate if these results apply to other data sets and other types of activation function. Furthermore, we aim to emphasize on the search of a more precise relation between the NMI and the redundancy of neurons.

#### ACKNOWLEDGMENTS

We wish to acknowledge the support of the Vicerrectoría Académica from Universidad de los Andes due the funding to this project by the program of research and creation credits.

- 
- [1] E. V. Garcia, T. L. Faber, C. C. David, and R. D. Folks, Computer analysis of nuclear cardiology procedures, in *Emission Tomography* (Elsevier, 2004) pp. 541–550.
  - [2] J. Gasteiger and J. Zupan, Neural networks in chemistry, *Angewandte Chemie International Edition in English* **32**, 503 (1993).
  - [3] J. Khan, J. S. Wei, M. Ringner, L. H. Saal, M. Ladanyi, F. Westermann, F. Berthold, M. Schwab, C. R. Antonescu, C. Peterson, et al., Classification and diagnostic prediction of cancers using gene expression profiling and artificial neural networks, *Nature medicine* **7**, 673 (2001).
  - [4] Y. Goldberg, A primer on neural network models for natural language processing, *Journal of Artificial Intelligence Research* (2015).
  - [5] J. Schmidhuber, Deep learning in neural networks: An overview, *Neural networks* **61**, 85 (2015).
  - [6] M. A. Nielsen, *Neural networks and deep learning*, Vol. 25 (Determination press San Francisco, CA, USA; 2015).
  - [7] R. Shwartz-Ziv and N. Tishby, Opening the black box of deep neural networks via information, arXiv preprint arXiv:1703.00810 (2017).
  - [8] N. Tishby and N. Zaslavsky, Deep learning and the information bottleneck principle, in *2015 IEEE Information Theory Workshop (ITW)* (IEEE, 2015) pp. 1–5.
  - [9] D. J. MacKay, *Information theory, inference, and learning algorithms*, Cambridge, Cambridge University (2003).
  - [10] J. V. Stone, Information theory: A tutorial introduction, arXiv preprint arXiv:1802.05968 (2018).
  - [11] F. M. Reza, *An introduction to information theory* (Courier Corporation, 1994).
  - [12] K. R. Ball, C. Grant, W. R. Mundy, and T. J. Shafer, A multivariate extension of mutual information for growing neural networks, *Neural Networks* **95**, 29 (2017).
  - [13] E. Schneidman, M. J. Berry II, R. Segev, and W. Bialek, Weak pairwise correlations imply strongly correlated net-

	1	2	3	4	5	6	7	8	9	10	11	12	13	14	15	16
16	0.060	0.005	0.019	0.018	0.023	0.012	0.036	0.013	0.016	0.032	0.051	0.020	0.001	0.021	0.000	
15	0.018	0.036	0.005	0.014	0.036	0.062	0.009	0.021	0.005	0.004	0.012	0.012	0.073	0.013	0.000	0.021
14	0.008	0.071	0.006	0.033	0.164	0.041	0.012	0.036	0.023	0.054	0.017	0.049	0.000	0.013	0.001	
13	0.034	0.022	0.027	0.028	0.050	0.049	0.011	0.070	0.020	0.025	0.055	0.000	0.049	0.073	0.020	
12	0.054	0.025	0.019	0.047	0.004	0.044	0.074	0.046	0.138	0.013	0.018	0.000	0.055	0.017	0.012	0.051
11	0.040	0.006	0.038	0.042	0.103	0.029	0.014	0.042	0.046	0.049	0.000	0.018	0.025	0.054	0.012	0.032
10	0.034	0.067	0.006	0.003	0.047	0.023	0.016	0.030	0.113	0.000	0.049	0.013	0.020	0.023	0.004	0.016
9	0.133	0.102	0.033	0.050	0.066	0.022	0.040	0.014	0.000	0.046	0.138	0.070	0.036	0.005	0.013	
8	0.036	0.032	0.024	0.059	0.076	0.006	0.103	0.000	0.014	0.030	0.042	0.046	0.011	0.061	0.021	0.036
7	0.066	0.025	0.074	0.077	0.024	0.045	0.000	0.077	0.040	0.016	0.014	0.074	0.049	0.012	0.009	0.012
6	0.003	0.023	0.047	0.011	0.017	0.000	0.045	0.006	0.022	0.023	0.029	0.044	0.050	0.041	0.062	0.023
5	0.004	0.012	0.013	0.051	0.000	0.017	0.024	0.076	0.066	0.047	0.103	0.004	0.028	0.164	0.036	0.018
4	0.030	0.009	0.025	0.000	0.051	0.011	0.077	0.059	0.050	0.003	0.042	0.047	0.027	0.033	0.014	0.019
3	0.059	0.010	0.000	0.025	0.013	0.047	0.074	0.024	0.033	0.006	0.038	0.019	0.022	0.006	0.043	0.006
2	0.063	0.000	0.010	0.009	0.012	0.023	0.025	0.032	0.102	0.067	0.006	0.025	0.071	0.036	0.060	
1	0.000	0.063	0.059	0.030	0.004	0.003	0.066	0.036	0.133	0.034	0.040	0.054	0.034	0.008	0.018	0.093

FIG. 5. Final local Normalized Mutual Information (NMI) for all possible pairs of neurons for the trained neural network with 16 neurons.

work states in a neural population, *Nature* 440, 1007 (2006).

- [14] Y. Lecun, L. Bottou, Y. Bengio, and P. Haffner, Gradient-based learning applied to document recogni-

tion, *Proceedings of the IEEE* 86, 2278 (1998).

- [15] D. P. Kingma and J. Ba, Adam: A method for stochastic optimization, *CoRR* abs/1412.6980 (2015).



# Noise, Information and Fitness in Changing Environments

Juan M. Pedraza<sup>1\*</sup>, David A. Garcia<sup>1,2,3</sup> and Muriel F. Pérez-Ortiz<sup>1,4</sup>

<sup>1</sup> Department of Physics, Universidad de los Andes, Bogotá, Colombia, <sup>2</sup> Department of Physics, University of Maryland, College Park, MD, United States, <sup>3</sup> Laboratory of Receptor Biology and Gene Expression, National Cancer Institute (NCI), National Institutes of Health (NIH), Bethesda, MD, United States, <sup>4</sup> Korteweg-de Vries Institute for Mathematics, University of Amsterdam, Amsterdam, Netherlands

## OPEN ACCESS

**Edited by:**

Luis Diambra,  
National University of La Plata,  
Argentina

**Reviewed by:**

Sungwoo Ahn,  
East Carolina University, United States  
Ignacio Enrique Sánchez,  
Consejo Nacional de Investigaciones  
Científicas y Técnicas (CONICET),  
Argentina

Daniel Polani,  
University of Hertfordshire,  
United Kingdom

**\*Correspondence:**

Juan M. Pedraza  
jmpedraza@uniandes.edu.co

**Specialty section:**

This article was submitted to  
Biophysics,  
a section of the journal  
*Frontiers in Physics*

**Received:** 26 March 2018

**Accepted:** 23 July 2018

**Published:** 17 August 2018

**Citation:**

Pedraza JM, García DA and  
Pérez-Ortiz MF (2018) Noise,  
Information and Fitness in Changing  
Environments. *Front. Phys.* 6:83.  
doi: 10.3389/fphy.2018.00083

In this paper we discuss recent results regarding the question of adaptation to changing environments in intermediate timescales and the quantification of the amount of information a cell needs about its environment, connecting the theoretical approaches with relevant experimental results. We first show how advances in the study of noise in genetic circuits can inform a detailed description of intracellular information flow and allow for simplified descriptions of the phenotypic state of a cell. We then present the different types of strategies that cells can use to respond to changing environments, and what a quantitative description of this process implies about the long term fitness of the population. We present an early approach connecting the transmission of information to the average fitness, and then move on to a full model of the process. This model is then simplified to obtain analytical results for a few cases. We present the necessary notation but avoid technical detail as much as possible, as our goal is to emphasize the biological interpretation and significance of the mathematical results. We focus on how carefully constructed models can answer the long-standing objection to the use of information theory in biology based on decision-theoretic considerations of the difference between the amount of information and its fitness value.

**Keywords:** bet-hedging, changing environments, gene noise, phenotypic variation, long term fitness

## INTRODUCTION

It has long been recognized that information about the environment is crucial for survival of all living things, and that a connection exists between long term environment and genotype and short term environment and phenotype. It has even been proposed that information storage and transmission is the fundamental feature of evolution [1]. Since evolution occurs via progressive changes in the genome, some information about the history of the environments the ancestors have faced must be stored in the genetic sequence [2]. On shorter timescales, a given genotype can result in different phenotypes through interactions with the environment and intracellular stochasticity. This can range from gene expression changes in bacteria in response to changes in the surrounding media, to the extreme differences in form and function between specialized cells in mammals. It follows that the phenotype of a cell has information about the current environment and/or the surrounding environment during development. Since selection happens at the level of phenotype, these two levels of information transmission and storage must be connected to the process of evolution. It therefore seems useful to quantify this flow of information in biological systems, which might allow for predictive calculations in a similar way to how optimizing the flow of mass and energy has advanced ecology [3].

Early attempts to use the formal definition of information [4] in biology ran into the following problem: every bit of information is in principle equally valuable in abstract communication channels, but for an organism some bits are more valuable than others. If there is a 50/50 chance that a predator is behind a bush, knowing for sure is a very useful bit, whereas knowing whether its left or right molar is bigger is a less useful bit. Since the meaning of each bit is irrelevant for the engineering problem of information transmission, many biologists thought that the amount of information was irrelevant and the important quantity was its decision-theoretic value [5]: the expected fitness given some particular information minus the expected fitness without it. In the predator-behind-bush example, presumably the best strategy (for the prey) under uncertainty is to leave the bush alone, incurring in a fitness cost in terms of lost food. With full information, half of the time the prey knows that the predator is not there and it can get the food and half of the time it has to run away, so on average he gets half of the food. In this case the value of the information on whether the predator is there or not is the fitness gain of half a bush worth of food, which is not in units of information. Unfortunately, quantifying this in principle would require an intimate knowledge of the fitness function and the dependence of phenotype on environmental cues. Furthermore, such calculations require knowing the fitness value of the wrong combinations of phenotype and environment, which are not easy to observe. For example, determining the value for a type of bird of knowing when the seasons come would require determining how it would do if it didn't migrate. For evolutionary timescales, this would mean knowing the maximum fitness it could have if it eventually adapted to not migrating. The fundamental difference between the information-theory approach and the decision-theory approach is one of the issues answered by the research reviewed here.

For the case of unicellular organisms, it is easier to both define and measure such quantities in laboratory settings. The possible environments for evolution can be defined experimentally [6], short term fitness is directly measurable from competition experiments [7], behavior can be controlled through genetic manipulation [8], and evolution experiments can be performed in human timescales [9]. A more tractable subset of the general problem of information flow in biology is then the quantifying of both the amount and fitness value of the information that a population has about a particular set of environments, and how it would evolve for intermediate timescales.

This question is related to another important problem in biology: how do cells adjust their expression pattern (phenotype) to respond to changing environments? It certainly involves the biochemical mechanisms through which a cell senses the environment and alters gene expression, but the question goes far beyond mechanistic responses. For example, it has been shown that under certain conditions it might be better for a cell not to try to determine precisely what environment it is facing but randomly switch between possible responses [10, 11]. This could be done blindly, but more generally, the response to external signals is increasingly found to be a combination of deterministic and stochastic parts that can result in changing

distributions of phenotypes, in what is known as a conditional, distributed or bet-hedging strategy [12]. This is equivalent to mixed strategies in game theory [13]. The possible strategies are sketched in Figure 1: assuming only three possible states of the environment and phenotype, matched by color, the distribution of phenotypes in the population for different environments is given by the bar graphs. In perfect sensing, the response is deterministic and simply changes to the appropriate state after some delay. In a purely stochastic strategy (blind switching), the cells are not measuring the environment and have a constant distribution. This means that for any change in environment some cells will already be in the new correct state but also that in any environment a sizable fraction is in the wrong states. For simplicity the figure ignores the important fact that growth differences would bias the distribution to the correct state, as will be shown in Figure 2, making it look like the distributions for conditional switching. In a conditional switching strategy, cells transition between states but with transition probabilities that depend on a measure of the environment, resulting in distributions that are biased toward the correct state but nevertheless always have some cells in the wrong state. These cells

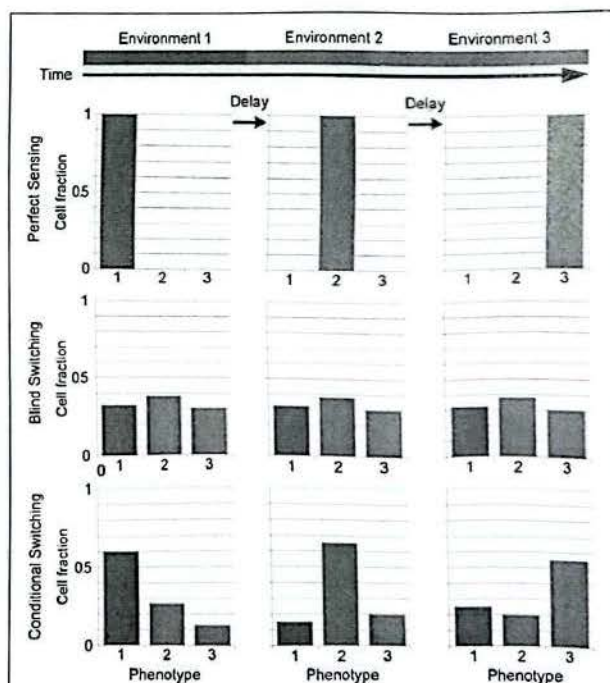


**FIGURE 1 |** Sketch of phenotype distributions corresponding to different strategies for adapting to fluctuating environments. In this example there are three possible environmental and corresponding phenotypic states. In perfect sensing, cells measure the environment and all change to the correct state. In blind stochastic switching, cells just try to maintain a distribution (which doesn't have to be uniform) regardless of environment. Here we don't show the important effect that growth differences would have, biasing the distribution to the correct state. In conditional stochastic switching, cells switch between states but with rates that depend on information from the environment and can bias it to the correct one even discounting growth effects.

are in a sense a “hedge,” or insurance in case the environment changes and the delay in changing accordingly is costly.

Given the inevitable stochasticity in intracellular processes [15], the cases where the response appears deterministic imply a noise reduction system [16, 17], whereas in many cases this variability is amplified and converted into a distribution of phenotypes [18]. A medically important example of this switching strategy is the phenomenon of bacterial persistence [19], where a very small fraction of a population switches on a timescale of hours in and out of a non-growing or slow-growing state that confers it tolerance against many antibiotics and other attacks. If the rest of the population is killed and the insult withdrawn, these cells can restore the population, but it is important to note that this new population is still susceptible to the insult, as opposed to the case where a genetic mutation confers resistance to the resulting population. The amount of cells in this persistent state does depend on the environment, but it is not simply a deterministic response to it, since a phenotype distribution including a persistent fraction is present before the insult [20]. This exemplifies the type of adaptation that will be discussed here.

## INFORMATION IN AN EVOLUTIONARY CONTEXT

A discussion on whether evolution can be profitably studied as an optimization process (illustrated by the discussions between Maynard-Smith [21] and Gould and Lewontin [22]) has raged on for 40 years between philosophers of biology. There are valuable arguments about the difficulty of defining an objective function (instantaneous individual fitness, inclusive fitness, long term population growth, evolutionary stability?), and other important points that remain under active research. Similarly, the use of information theory in biology has a long history of ardent proponents [1, 23] and detractors [24, 25].

However, a large group of researchers has simply sidestepped the discussion by profitably using optimization and information theory in various fields, from sequence analysis [26] to neural coding [27]. In particular, the recent availability of sequence data has allowed the direct comparison of information theoretic limits with actual observed distributions of sequences in particular contexts [28, 29]. It has even been proposed that information processing constitutes a driver to increasing organismal complexity [30]. Adami [31] has written a very readable account of the use of information concepts in evolutionary biology. Another field where information theory has found great success is neuroscience, where it is nowadays an essential tool; a good review is given by Dimitrov et al. [32]. Such breadth of fields using information theory has led to competing definitions of information for different situations, including mutual information [4], directed information [33], Fisher information [34], and others. While each has advantages, we focus on mutual information, which has important theoretic advantages [35] although directed information will make an appearance later on. It is also important to note that while we focus on prokaryotic gene expression noise for simplicity,

phenotypic differences depends not only on gene expression but also on protein states [36] and localization [37] and on epigenetic markers such as methylation [38]. The approaches worked out here will still hold for these other mechanisms, although the details of the calculations of noise and information will vary; see for example Cheong et al. [39], Thomas and Eckford, [40], or Micali and Endres et al. [41]. We also leave aside the long term relation between sequence and selection, although it underlies the assumptions of near optimality.

## THE ROLE OF NOISE

What has changed in the meantime is our knowledge of noise and dynamics in intracellular circuits and our experimental tools to probe them. We have an ever growing collection of data and models which provides examples for many types of circuits in different organisms [42]. We have a rough description of the processes that lead to cell specialization in many multicellular organisms [43, 44]. We have detailed models and measurements of the way stochasticity arises in intracellular circuits [15, 17] and how it can result in phenotypic variability [45, 46]. Experimentally, we have measurements at the single molecule level of mRNAs and proteins [47, 48], single cell transcription data [49, 50], and automated ways to observe populations [6] and single cells [51] in changing environments over long periods. We also have the tools of synthetic biology to probe and manipulate circuits [52, 53], and the methods of experimental evolution [9] and competition [7] in unicellular populations. This detailed knowledge of the noise allows us to compute directly the information content of various biochemical processes. In the next section we will see the example of a single gene, but many other examples have been worked out.

An objection showing up as late as 1997 to the use of information theory in biology was that biology was not stochastic enough [54]. The underlying argument is that if signaling happens through molecules, their numbers are so high that interactions are essentially nonrandom processes. Quantitatively, one could expect that a typical signaling protein with numbers of the order of 10000 would have fluctuations of the order of  $\sqrt{10000} = 100$ , resulting in a relative noise (coefficient of variation) of 1%, and making a probabilistic description unnecessary. This is misleading not only because there are many relevant situations where the number of signaling molecules can be  $< 1$  [55], but also because we now know that the most relevant noise in protein level does not come from the fluctuations in the number of proteins itself but in that of the mRNAs that produce it [11], the binding and unbinding of transcription factors that control it [56], and the fluctuations transmitted from other parts of the cell [57, 58]. This means that noise in genetic circuits is large and ubiquitous, and that a detailed description of their dynamics should include its probabilistic aspects.

We have also learned about the effect of feedbacks in genetic circuits, where they can be used to reduce fluctuations or amplify them [59, 60], and can generate metastable states and multimodal distributions [59]. These in turn correspond to different phenotypic states, and in some cases we know how the

distribution of states is determined and how to manipulate it [61]. So we now have mechanistic knowledge, in a few cases, of how phenotypic diversity is generated and maintained. Conversely, since those states are in general maintained by the dynamics of noisy genetic circuits, they are susceptible to error and any memory contained within them is limited and imperfect [62]. Therefore if we are interested in how cells adapt to changing environments, we need to know how much information a cell can actually store about the environmental history and how much information can actually be transmitted from the environment to intracellular circuits in the presence of noise.

## INFORMATION CONTENT OF GENE EXPRESSION

Tkačik et al. [63] utilize analytical, approximate models of noise in gene expression to determine the channel capacity of a gene, which is the maximum rate of information transmission for a single gene under various conditions. In particular, they look at transcription factor binding and unbinding and the intrinsic noise of gene expression and show that the capacity of a single regulatory element is 1 bit under typical conditions and that under reasonable but more restrictive assumptions it can increase to around 3 bits. This has important implications for biology: the first point validates the use of Boolean networks, a popular approximation to genetic networks, in many cases. The second illustrates that although protein levels are usually on the order of thousands, the reliable transmission of more than a few levels is limited by the stochasticity in the system and parameters need to be carefully tuned to achieve it. In the particular case of the design of synthetic circuits, the need for proper impedance matching has already been noted [64], but the results of Tkačik et al. show that the stochastic effects also need to be properly tuned.

Following their notation, we look at a single gene controlled by a single transcription factor. Let  $g$  be the level of expression of the gene (in a simple case, the protein number) and  $c$  the amount of transcription factor.  $c$  corresponds to the input signal, which can have a distribution  $p_{TF}(c)$ . If gene expression were deterministic, there would exist a function  $g^*(c)$  that directly mapped input level to expression. Since gene expression is stochastic, this situation is described through  $p(g|c)$ , the conditional probability of observing expression  $g$  given input  $c$ . Later we will explicitly incorporate the time dependence. With these definitions, we can look at information theory quantities such as the mutual information between the input and output distributions. Using  $p(g,c) = p(g|c)p_{TF}(c)$  and  $p_g(g) = \sum_c p(g|c)p_{TF}(c)$  the mutual information would be

$$\begin{aligned} I(g, c) &= \sum_{g,c} p(g, c) \log_2 \left( \frac{p(g, c)}{p_g(g)p_{TF}(c)} \right) \\ &= \sum_{g,c} p(g|c)p_{TF}(c) \log_2 \left( \frac{p(g|c)}{p_g(g)} \right) \quad (1) \end{aligned}$$

where the logarithm is in base 2 to obtain units of bits, and we have used  $g$  and  $c$  for both the random variables and their

distribution to simplify the notation. Here we can see more precisely what we meant by "tuning the stochastic effects": "if the gene expression is to respond with many distinguishable levels, the distribution of transcription factors cannot be arbitrary. For example, a gene with a step response curve could pass no information if the corresponding transcription factor distribution was zero on one side of the threshold. More realistically, a gene with a sigmoidal response curve could transmit more information if the corresponding transcription factor had a distribution proportional to the slope of the response curve than if it had a bimodal distribution.

This approach seems to imply that the system is maximizing the amount of information transmitted. A simple example to the contrary is the case of a binary output, where the cell only needs to precisely transmit the information of whether a certain threshold has been crossed and respond by fully turning on a gene. In this case, the information lost far from the threshold is irrelevant, and a bimodal distribution of inputs would be best. It is important to distinguish two possible issues: one is that not all information might be relevant, and the other is that the evolutionary value (or decision-theory value) of information is not the same as the amount of relevant information. The issue of how much information is actually useful for prediction has been largely solved by the "information bottleneck" method proposed by Tishby et al. [65], where they show how to determine the amount of relevant information a variable has for any particular prediction goal. In the present discussion, what the goal is needs to be quantified using the fitness. We will later return to this point to show how to account for the fitness value of the transmitted information. But first, we need to determine what exactly we mean by fitness for the cases of interest.

## SENSING VS. GUESSING AS A STRATEGY

Real environments are a mix of predictable and stochastic characteristics. Cells have different ways of managing their phenotypes/strategies to adapt, including systems that allow the prediction of the reliable parts such as circadian clocks, sensing mechanisms such as chemotaxis, and bet-hedging strategies such as the phenomenon of bacterial persistence explained above. While the possibility of bet-hedging as a strategy had been analyzed before [11, 66, 67], it is in the work of Kussell and Leibler [68] that we find a framework that captures the full range of possibilities. An idealized extreme would be to have perfect sensing, where the cell would respond to an environment  $s$  (described in general by a vector) with the gene expression pattern  $g$  that gives the highest fitness  $f(g, s)$  in that environment,  $g^*(s)$ . Perfect sensing is impossible, but even imperfect sensing has a metabolic cost, which must increase with the accuracy of sensing. For example, the noise of ligands binding and unbinding from their receptors can be ameliorated by averaging over more receptors, but those cost energy to produce and recycle. Additionally, there is an unavoidable delay between measurement and response, which in principle can be reduced but again at a metabolic cost [69]. So even in the case of direct sensing there is a tradeoff between the fitness cost of

responding late and sometimes wrongly and the fitness cost of increased metabolic load. Note that this description implies that the quantity to be optimized is not the instantaneous fitness  $f(g,s)$  but the long term average growth for a sequence of environments.

At the other extreme the idealized case is that of a completely stochastic response: a population that generates large phenotypic variability so as to cover the different possible environments. It can be easily implemented by a positive feedback tuned to amplify noise to produce broad or multimodal distributions of expression [59]. This strategy has some advantages: since the possible state of the environment is given by multiple variables, some of which are continuous, there are infinite possible environments. It then becomes impossible to have sensors for every case, and unfeasible even to have enough to precisely determine the set that would correspond to each possible phenotypic state. Another important effect is that if the switching is slow compared to the environment, a bigger fraction than determined by switching alone will be in the correct state simply because they grow faster. But since there is a fraction of the population that will always have suboptimal fitness, this strategy would seem in principle to be inferior to (imperfect) sensing. By explicitly taking into account the cost of sensing and the disadvantages of delay in a simplified situation, Kussell and Leibler show the range of cases where pure stochasticity surpasses sensing as a strategy. One situation in particular gives the advantage to bet-hedging: cases where there are states of the environment that are rare but rapidly lethal for the wrong phenotype, such as for bacteria in the presence of antibiotics. In this situation, preemptively having a small fraction of the population in a state that can survive in the presence of antibiotics can be advantageous even if those cells are at a big disadvantage in other environments.

The general case is one where the system responds stochastically, but with the probabilities of transition between phenotypic states influenced by what is sensed of the environment. This is the case, for example, in bacterial persistence. While Kussell and Leibler mentioned it as a conjecture, we know now that the rates of transition into and out of the persistent state depend on the media: the probability of going into the persistent state increases if the cell is stressed [70] (for example, by antibiotics) and the probability of coming out increases in rich media. It is important to note that this does not imply that persistence occurs only as a response to stress; it was shown by Balaban et al. that cells enter the persistent state before the stress is applied [20]. It is the probability of going into the persistence state that changes.

Clear experimental evidence for the viability of the stochastic switching strategy comes from the experiments of Acar et al. [14]. They engineered two strains of *S. cerevisiae* to stochastically switch the gal operon on and off at different rates, but with the *URA3* gene under its control. This gene was used because it allows for both positive and negative selection: when the media contains no uracil, cells that express *URA3* have an advantage, but when the media contains both uracil and 5-fluoroorotic acid (5-FOA), this small molecule is transformed by the *URA3* protein into a toxic compound that gives a disadvantage to the cells that express it but no disadvantage to those that do not. By comparing the

growth rates of the strains in media that alternated with different rates between media without uracil and media with uracil and 5-FOA, they found that the strain with fast switching had a faster average growth rate than the slow switching strain in fast switching-media and vice versa.

This experiment is very illustrative for the present discussion for various reasons. If we ignore the time dependence, the slow switchers and fast switchers are simply bet-hedging with different distributions, as can be seen in Figure 2A. In nonselective media there are cells with very different levels of gene expression, and the two clear peaks in the distributions represent the two possible states. Figure 2B shows the distributions of expression after 4 days in media without uracil (environment  $S_1$ ) and Figure 2C shows the distributions of expression after 4 days in media with uracil and 5-FOA (environment  $S_2$ ). Although they have no direct sensing of the two environments, the fact that only the correct phenotype can grow results in very skewed distributions in selective media. Note that in both cases the fast switchers have a larger fraction that is not in the correct state (the red tails), and this results in slower growth after some time in either environment but also on an initial advantage after a media change (Figures 2D,E). This happens because the fraction of cells in the wrong state after a long time in an environment is also the fraction of cells that are already in the correct state when the environment changes. However, in repeatedly changing environments the winner depends on the speed of change. If the environment changes every 40 min, the fast switchers have a long term advantage because in the time it takes the slow switchers to switch, the fraction of the fast switchers that was "wrong" has been already growing (Figure 2F). If the environment changes every 100 min the slow switchers have the advantage because they spend longer in the situation where they have the advantage (Figure 2G). While the differences are small for the cases shown, they are amplified exponentially and result in measurable differences in average growth rate. This shows that the instantaneous fitness  $f(g,s)$  is not necessarily what is optimized by evolution, but perhaps its long term average over the population is [71–73]. This can be visualized as the red and blue shaded areas in Figures 2F,G representing the cumulative growth advantage of each strain. For rapidly changing environments the total of the red areas is larger than the blue, and conversely for the slowly changing environments.

Since this system was artificial in its construction and the possible states of the environment, it approached the idealized limit of bet-hedging. However, the media was changed periodically rather than randomly. In natural cases of adaptation to a periodically switching environment cells can adapt over evolutionary timescales by developing a matching internal clock, but one that is not completely independent of the environment so that it can be entrained to avoid phase drift [74, 75]. However, it is easy to see that if the environments were changed randomly with average times close to those used in the periodic cases the main effect would still hold: cells that switched with rates matching the environment would have an advantage over those that switch with the wrong rates. Their system thus illustrates a question that will be answered more generally later: if the cells will adopt a distribution of phenotypes without measuring the

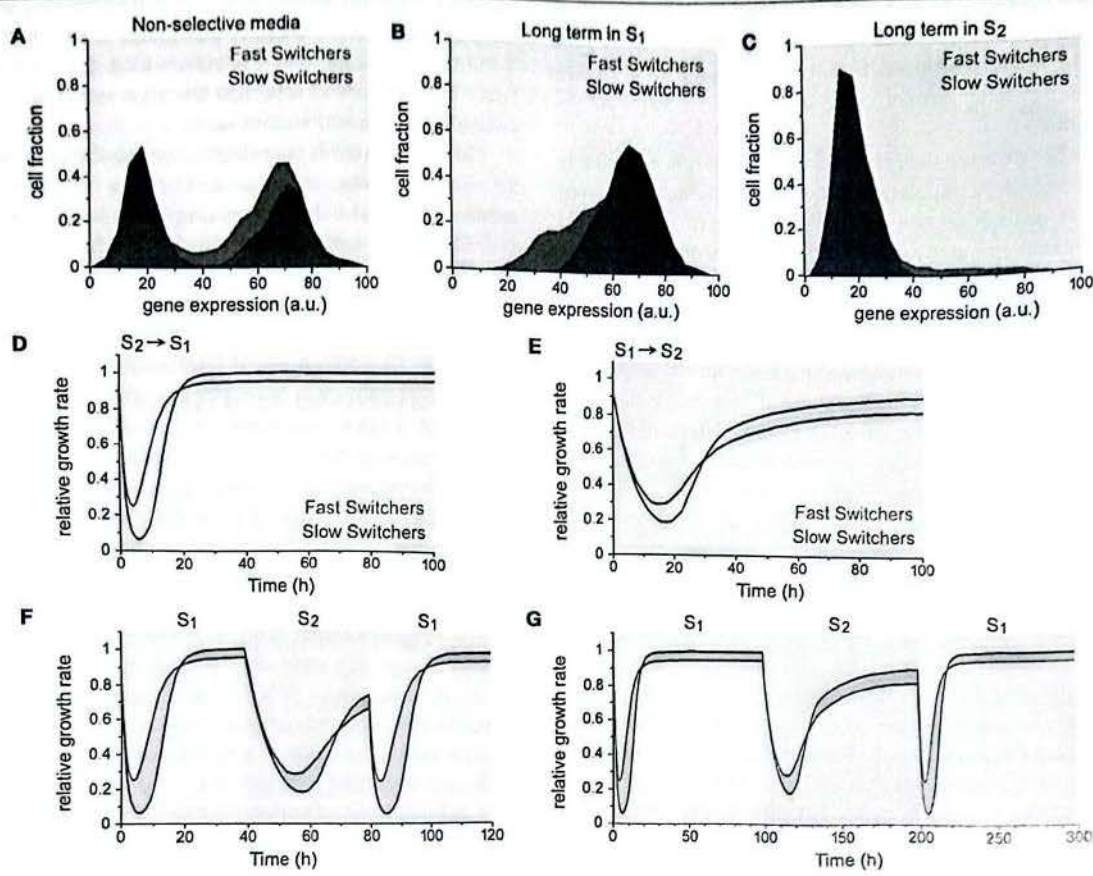


**FIGURE 2 |** Long term growth in a bet-hedging strategy. **(A)** Long term distribution of phenotypes (gene expression) for the slow switchers (blue) and fast switchers (red) in nonselective medium. Cells have mostly either high (ON) or low (OFF) expression. **(B)** In media without uracil (environment S1), only cells that are ON can grow, but the distributions are wide because cells are still switching. The distribution of fast switchers is wider because of a faster stream of cells switching off, resulting in a larger fraction of cells in the wrong state (red tail). **(C)** Conversely, in media with uracil and 5-FOA (environment S2) only OFF cells can grow, but the distribution is still wider for the fast switchers. **(D)** When changing from a long time (4 days) in S2 to S1, cells have low growth until the ON fraction grows. After some time, the slow switchers grow faster, because of the different fractions in the ON state shown in **(B)**. **(E)** When changing from a long time (4 days) in S1 to S2 cells have low growth until the OFF fraction grows. Again after some time, the slow switchers grow faster. **(F)** If media are alternated every 40 min, this results in longer periods where the fast switchers grow faster than the slow switchers, leading to higher average growth. The total advantage can be visualized by the areas shaded in red vs. the areas shaded in blue. Intuitively, if the time is short the initial advantage of the fast switchers exceeds the eventual advantage of the slow switchers. **(G)** The opposite happens if the period is changed to 100 min. Adapted from Acar et al. [14].

environment, how do they choose the distribution of phenotypes that maximizes their fitness?

## OPTIMIZATION OF AVERAGE FITNESS UNDER INFORMATION CONSTRAINTS

In the context just explained of a finite set of possible environments and a set of possible phenotypes, but taking into account the stochasticity mentioned before, it is possible to properly define one of our original questions: given the full fitness  $f(g, s)$  for all possible states of gene expression and environment, what is the best possible  $p(g|s)$ ? The ideal  $g^*(s)$  can be directly obtained from  $f$ , but since the cell cannot measure  $s$  nor maintain  $g$  with infinite precision the most it could do is optimize the conditional distribution  $p(g|s)$ . But why not simply

make it as narrow a peak as possible around  $g^*(s)$ ? Notice that the metabolic costs mentioned before would in principle go into the state  $g$ , but that makes the question somewhat tautological. We must be clear about the timescales and genes under study; as Maynard-Smith noted, we cannot be sure that the optimum has been achieved and what the physical limitations involved are in general, but optimization is a useful heuristic for a limited system. In this case, this means limiting the timescale of study to changing levels of gene expression and perhaps protein affinities rather than the evolution of an entirely different sensing system, and the genes to a particular set directly involved with the response to a particular characteristic of the medium. The disadvantage of this approach is that metabolic costs are hidden in the fitness function; perhaps they can be taken into account by explicitly including the energy needed for a particular sensing and expression control system. This would be a strong simplification,

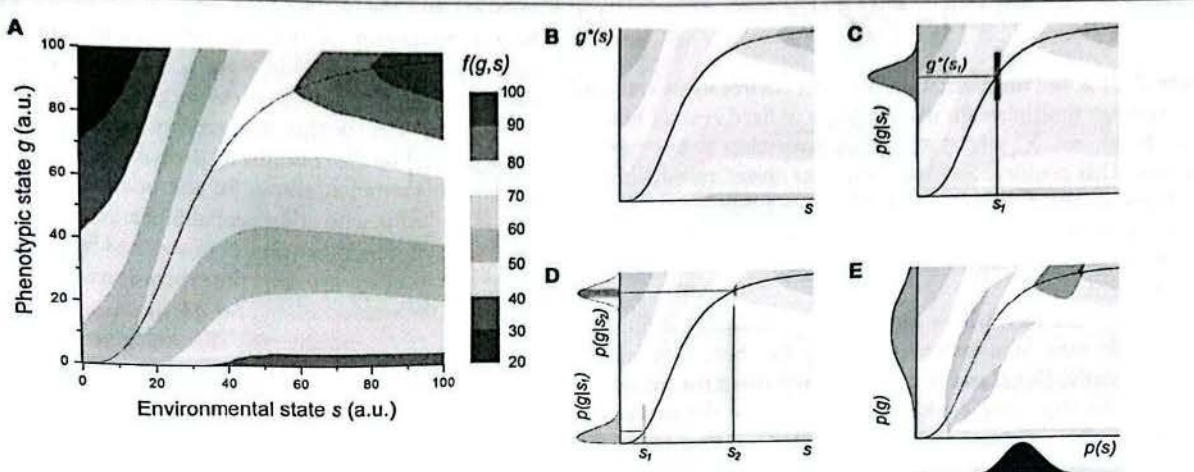


**FIGURE 3 |** Graphical representation of the definitions. **(A)** Height map of a possible fitness function  $f(g,s)$  (as percentage of the maximum) of one dimensional environmental state and phenotypic state in arbitrary units. Inspired by Taylor et al.’s analysis [76] of Dekel and Alon’s data [77]. **(B)** The function  $g^*(s)$  is given by the phenotypic state with the highest fitness for each environmental state. **(C)** Because of intracellular stochasticity, even a fixed known environment can result in a distribution of phenotypes, given by  $p(g|s)$  (gray). The mean would not need to lie exactly on  $g^*(s)$  because  $f(g,s)$  can drop off asymmetrically, and evolution would optimize  $\langle f(g,s) \rangle$  (colored rectangle). **(D)** The shape of the distribution of phenotypes can change for different reasons: The noise in the distribution tends to increase with increasing mean for statistical reasons, but the pressure to reduce the width can vary (in this case, increase) with the curvature of  $f(g,s)$ . This is represented by the colors indicating the fitness within the distribution. **(E)** If the environment also has a distribution,  $p(s)$  (black), the convolution of all  $p(g|s)$  with  $p(s)$  gives the total distribution of phenotypes,  $p(g)$ . Note that this doesn’t mean that  $p(g,s)$  is just the multiplication of probabilities, but its shape will be determined in part by  $f(g,s)$ . In this case  $\langle f(g,s) \rangle$  corresponds to the height in the colored region, integrated with weight  $p(g,s)$ .

which would only make sense if the way the fitness function was computed in the first place was through a balance of energies.

Taylor et al. [76] solve this problem by using the information concepts explained before. They group the factors that would incur a metabolic cost into the mutual information between  $g$  and  $s$ , and propose that the optimization be done maximizing the average fitness for a given mutual information, or conversely minimizing the mutual information needed to achieve a given level of fitness. In this view,

$$I(g,s) = \sum_{g,s} p(g|s) p(s) \log \left( \frac{p(g|s)}{p_g(g)} \right) \quad (2)$$

and

$$\langle f(g,s) \rangle = \sum_{g,s} p(g,s) f(g,s) = \sum_s p(s) \sum_g p(g|s) f(g,s) \quad (3)$$

where for simplicity we omit the vectorial notation. The last expression has a clear biological interpretation: averaging over the possible states of the environment (externally determined), then for each particular environmental state averaging over the possible responses of the cell to that environment (determined by the genes under study) of the fitness function (determined by the relevant biochemistry). These definitions are illustrated schematically in Figure 3. The fitness function  $f(g,s)$  for a one dimensional environmental state  $s$  and phenotypic state  $g$  can be represented as a heat-map (Figure 3A). The ideal phenotype  $g^*(s)$  would be the maximum of this function for each possible value of  $s$  (Figure 3B). Even in a fixed environment  $s_1$ , noise in

the sensing systems and in gene expression prevents the cells from knowing  $g^*(s_1)$  precisely and maintaining a particular level of expression, resulting in a distribution of expression  $p(g|s_1)$  (Figure 3C, in gray), in principle centered on  $g^*(s_1)$ . Note that the shaded area in the heat map represents the average fitness for a single cell or the total fitness for a population with the given distribution of expression. The distribution of expression is in general not symmetric, nor is the slope of  $f(g,s_1)$  around  $g^*(s_1)$ . If the population is optimizing the total fitness, but is constrained by the noise, it could in principle still shift the shape and position of the distribution within some constraints. For different values of  $s$  the optimal shape of the distribution would be different, as shown in Figure 3D. This can be further complicated by the fact that the environments the cell encounters also have a distribution  $p(s)$ , shown in Figure 3E in black. Note that the resulting distribution of phenotypes  $p(g)$ , shown in Figure 3E in gray, is not simply the projection of  $p(s)$  through the function  $g^*(s)$ . As the colors in Figure 3D show, it is more costly in fitness terms to deviate from the optimal value around  $g^*(s_2)$  than around  $g^*(s_1)$ . This means that the resulting optimal distribution will depend on the entire range of  $f(g,s)$ . The colored area in Figure 3E corresponds to the support of  $p(g,s) = p(g|s)p(s)$ , and  $\langle f(g,s) \rangle$  would correspond to the sum of the fitness values in this area weighted by  $p(g,s)$ .

The problem is thus reduced to an optimization under constraints which can in principle be solved through variational calculus. Intriguingly, when posed in this form the problem has a formal solution reminiscent of a familiar result from statistical mechanics:

$$p(g|s) = \frac{p(g)}{Z(s)} e^{\lambda f(g,s)} \quad (4)$$

where  $Z(s)$  is the normalization for each environment and  $\lambda$  is the Lagrange multiplier for the condition of fixed average fitness. Since  $p(g) = \sum_s p(g|s) p(s)$ , this expression is an implicit solution. This problem has been solved as one of rate distortion functions in the field of communications [78]. However, this still requires an explicit form for the fitness function, which is difficult to obtain even for single variables for the gene and the environment.

There is one case where the fitness, functionally defined as the growth rate in a bacterial culture, has been determined experimentally. Dekel and Alon [77] manipulated the lac operon of *E. coli* so that they could externally induce the expression independently of the lactose in the media. They then tested the growth rate at multiple combinations of gene expression and media, and thus from their data the fitness function  $f(g,s)$  can be obtained [76] in terms of the particular  $g$  (expression of the lac operon) and  $s$  (lactose concentration in the medium). It should be noted that this is not the long term limit for changing media as described before but simply the growth rate in a particular environment. Additionally, from their fitness they obtain the optimal expression  $g^*(s)$  and show that over relatively short times of about 400 generations in a constant medium cells adjust their average expression to this level.

## A FULL MODEL OF ADAPTATION

A difference between the approaches explained so far is that in one case the input is an intracellular signal  $c$  and in the other the conditioning variable is the actual state of the environment  $s$ . In reality a cell cannot optimize  $p(g|s)$  since it must work with its perception of the environment, so at least for the timescales of interest it can only optimize  $p(g|c)$ , where  $c$  is a variable that correlates imperfectly with the environment. What  $c$  depends on the particular case, and depends mostly on what we define as the system of interest. For example, in the case of chemotaxis in *E. coli* the environmental signal of interest  $s$  is the local concentration of a given small molecule, but the only information the cell has access to is the occupancy level of receptors for that molecule. While clearly correlated, these two quantities are not the same. Furthermore the expression of those receptors is under control of the cell, so  $c$  could vary from cell to cell in the same environment  $s$ . All of this needs to be included in a full model.

The effect of delays and memory, or more precisely, the fact that the current state of the cell can depend on previous states of itself and the environment should also be included. Their importance was shown experimentally by Lambert and Kussell [79], who measured the growth rates of *E. coli* in media that switched periodically between lactose and glucose as the carbon source, and confirmed that the growth rate even after changing media depended on what the cell had been exposed to before, in some cases almost a generation earlier.

A model incorporating all of these aspects is constructed by Rivoire and Leibler [73]. We present it in a hybrid of their

notation and the one we have been using so far. Let  $p(s_t|s_{t-1})$  be the probability of finding the environment in state  $s_t$  at time  $t$  given that it was in state  $s_{t-1}$  in the previous time. The discretization of the time works in general, but the underlying assumption here is that the environment is Markovian. Let  $\pi(g_t|g_{t-1}, c_t)$  be the conditional probability we had been calling  $p(g|c)$ . This notation allows for the possibility of memory and avoids confusion with other probabilities. This is the part that will be optimized, and it is strongly constrained by any details known about the circuits controlling the expression of the relevant genes, including their stochasticity. Let  $q(c_t|g_{t-1}, s_t)$  be the probability of having  $c_t$  as the internal variable given that the state of the environment is  $s_t$  and the previous state of the cell was  $g_{t-1}$ . This allows for each cell to receive different information from the environment and have different internal representations of it; in the example of chemotaxis,  $g_{t-1}$  would include the amount of surface receptors present. Finally, the fitness  $f(g_t, s_t)$  is interpreted as the expected number of descendants in the next generation given expression  $g_t$  in environment  $s_t$ . This is a stochastic process in itself. In this notation, a very general model of adaptation to changing environments can be constructed as shown in Figure 4A. The objective function for optimization would be the asymptotic growth rate of the total population size [71],  $\Delta_{p,f,q}(\pi) = \frac{1}{t} (\log |N_t|)$ . This corresponds to the Lyapunov exponent in dynamics. Biologically, it can be understood as the growth rate of all cells in the population averaged over different time histories of the environment, for times that are long compared to the average time spent in a particular environment. It is a delicate definition, since the average depends on the statistics of the environmental states, but for reasonable conditions it can be shown to exist. Care should be taken when using it in more general cases, as when taking mutations explicitly into account. With this definition, the optimal strategy is simply the conditional probability  $\hat{\pi}(g_t|g_{t-1}, c_t) = \text{argmax } \Delta_{p,f,q}(\pi)$ , which is the part that the cell can control.

Note that despite its generality this model does not include the possibility of the environment depending on the actions of the cells. This is an important omission, as it excludes for example a normal growth curve where the media changes with cell activity as well as cases like chemotaxis, where changing the local environment is the function of the circuit. This point is exemplified in the famous evolution experiments of Lenski and Travisano [9] where a population cell is evolved over thousands of generations in media that changes daily through depletion by the population and subsequent reinoculation in fresh media. As shown in detail in similar experiments by Oxman et al. [80], shorter lag times appear earlier than faster growth rates, because it doesn't help to be able to grow faster if in the meantime a competing mutant has depleted the media. This kind of effect could not be predicted by the present model.

## ANALYTIC SOLUTION FOR A SIMPLIFIED MODEL

The full model cannot be solved in general, but Rivoire and Leibler follow a very meticulous procedure of starting with

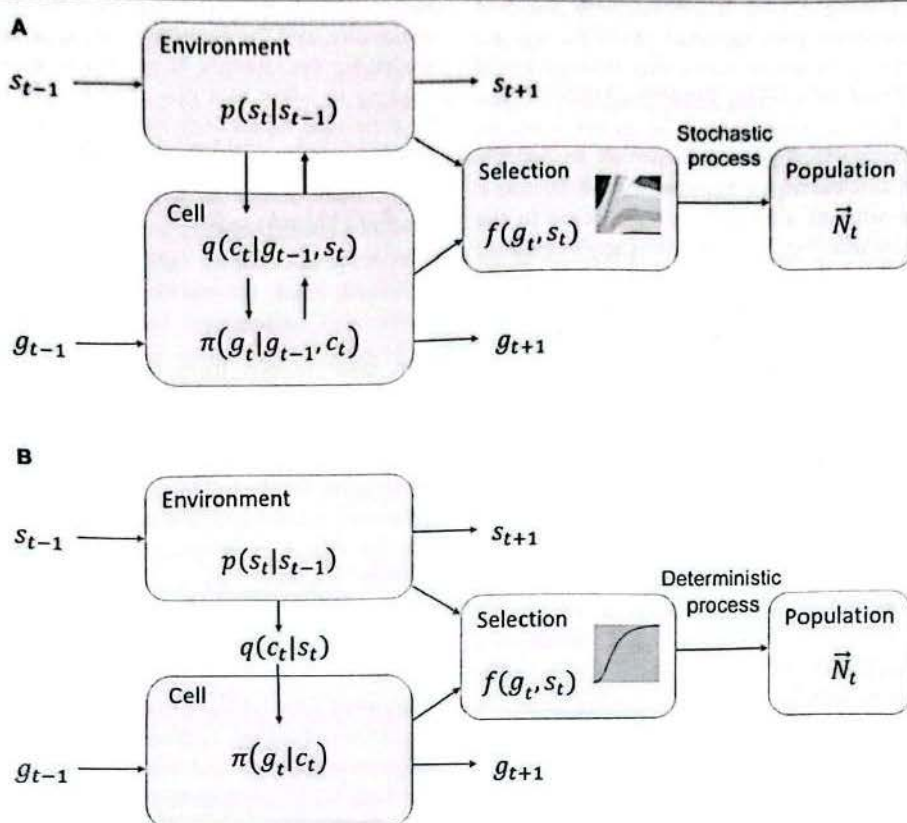


**FIGURE 4 |** Schema of the models for a cell's response to changing environments. **(A)** Full model as described in the text. Note the black arrow, which represents the possibility that the cells will change their environment. **(B)** In the simplified system, all cells receive the same information from the environment, independently of their state. Cells have no memory, the instantaneous fitness is a multiplication factor rather than a probability and it is 0 except for one phenotypic state per environment. Based on Rivoire and Leibler [73].

multiple simplifying conditions to obtain a simple analytical result and then exploring the consequences of successively lifting some of those conditions. The main insights from a simplified model were obtained previously by Donaldson-Matasci et al. [72], in an engaging article where they emphasize the parallels with the use of information theory in ecology. We present them in the context of the full model because it makes the conditions and limitations of the simple model clearer.

The first condition is that the stochasticity in reproduction is ignored, so that  $f(g_t, s_t)$  is simply the number of descendants in the next generation for a cell of phenotype  $g_t$ . This greatly simplifies the definition of the long term growth rate of the population, which will determine the objective function of the optimization, but explicitly excludes the possibility of extinction. The second simplifying condition is that cells have no memory,  $\pi(g_t|g_{t-1}, c_t) = \pi(g_t|c_t)$ . This excludes the long term maintenance of subpopulations as in the case of persistence or differentiation. The third simplifying condition is that the information that can be obtained from the environment is the same for all cells,  $q(c_t|g_{t-1}, s_t) = q(c_t|s_t)$ . This excludes the possibility of cells controlling their sensing mechanisms through feedback as in chemotaxis. The fourth simplifying condition

is that there is the same number of possible states for the environment and the cell, with only one phenotypic state per environment where cells can grow,  $f(g_t, s_t) = 0$  except for a single pair  $(g_t, s_t)$  per environment. We call  $s_g$  the environment corresponding to a given phenotype in these pairs. While clearly non-biological, this last condition is necessary for obtaining simple analytical solutions and could in principle be lifted at the expense of cumbersome calculations without changing many of the insights from the paper. Note also that using a discrete, small number of phenotypic states is justified by the results of section Information Content of Gene Expression. The system described by all of these conditions is a much simpler one, summarized in Figure 4B.

Our initial questions can be fully answered in this simplified model: the best strategy in this case is given simply by Bayesian inference. If the only information a cell population had about the environment was the steady state distribution  $p(s)$ , the best strategy would be proportional betting [81]: to assign the phenotypic states proportionally to the probability of the corresponding environmental state,  $\hat{\pi}_0(g) = p(s)$ . A classic example is betting on horse races: if you know the probability of winning for each horse and assuming proportional payoffs,

you might consider betting all on the horse with the best chance. That would maximize your expected payoff for a single game. But if you want to play many times, that strategy would result almost certainly in you losing everything after a few races. A better long term strategy would be to bet a bit on the other horses to ensure that you can't lose all in a single game. But you would not bet equal amounts on all horses; if the odds are fair the amount should be proportional to the chance each horse has of winning. This intuition was formalized by Kelly [81], who showed that not only is proportional betting the optimal strategy even for unfair odds but that using it your money would grow exponentially with a rate limited by the amount of information you have about the horses.

When a signal  $c_i$  is present, the cells can estimate better the current state of the environment, and the best guess for each state is given by a Bayesian estimate, giving rise to conditional proportional betting,

$$\hat{\pi}(g|c) = \frac{p(s_g) q(c|s_g)}{q(c)} \quad (5)$$

where  $q(c) = \sum_s q(c|s)p(s)$ . As the authors point out, this problem has close equivalents in finance and other areas. In the horse race example, this would be equivalent to knowing that the probabilities of each horse winning depend on the jockeys, so you would adjust your bets every race depending on the current jockeys. In both cases mentioned, the cells need to have knowledge of the steady state distributions. If that information can be genetically encoded, the optimization of the long term growth rate insures that evolution would select the mutants with the encoded distribution closest to reality. It is in this sense that evolution can be thought of as the long term process of encoding information about external conditions in the DNA.

The second question, about the value of information, can also be directly answered here: since those two strategies correspond to the best possible outcomes with and without information about the environment, the difference in the objective function is the value of the information acquired. In this case

$$\Lambda_{pf,q}(\hat{\pi}) - \Lambda_{pf,0}(\hat{\pi}_0) = I(c,s), \quad (6)$$

the mutual information. While this is valid only for an oversimplified model, it is remarkable that the issue mentioned in the introduction about the difference between the amount of information and the value of information completely disappears: they are in this case the same.

In the paper, Rivoire and Leibler obtain various corrections for this result, usually as bounds, when the simplifying assumptions are relaxed, moving back toward the full model. Two points in particular are worth mentioning here: the first is that allowing cells to have memory changes the relevant quantity from the mutual information to the directed information. The second point is that while the calculations presented here compare optimal strategies under different amounts of information, the formalism permits the calculation of the cost of using a suboptimal strategy  $\pi$ . This is important because as mentioned

before, there's no guarantee that the population has attained optimality, and for evolutionary experiments it would be useful to predict the changes in growth rate as the cells change their strategy to adapt to a new medium. Remarkably, this cost can be expressed as another information theoretical quantity, the relative entropy or Kullback-Leibler divergence [82]:

$$\begin{aligned} \Lambda_{pf,q}(\hat{\pi}) - \Lambda_{pf,0}(\pi) &= D_{KL}(\hat{\pi}||\pi) \\ &= - \sum_{g,c} \hat{\pi}(g|c) \log \left( \frac{\pi(g|c)}{\hat{\pi}(g|c)} \right) \geq 0 \quad (7) \end{aligned}$$

The main insight from these results is that under certain conditions the decision theoretical value of information in an evolutionary context can be written explicitly in terms of information theoretical quantities. While no equivalent analytical result exists for the full model, it seems plausible that the conflict between the information theory and decision theory approaches can be solved by a quantitative model with the long term population growth rate as the function to be optimized.

## DISCUSSION AND OUTLOOK

The use of information theory tools has been profitable in many branches of biology, and advances in the study of stochasticity in gene expression and microbial growth have provided new test beds for its applicability. Fundamental questions about how organisms manage information on their environments and how evolution can optimize their strategies to respond to uncertain environments can be posed in a more limited but better defined form as they apply to the growth of microorganisms in changing media. This allows precise mathematical formulations that can provide general insight as well as providing experimental means of testing those predictions. In this context, one overarching doubt about the applicability of formal measures of information to situations where the semantic content of a message should be paramount is elegantly resolved by showing an explicit connection between the information theory measure and the decision-theory value of information. Furthermore, increasing numbers of experimental studies are allowing ever more precise questions to be asked and the generality of any claims to be directly explored.

Despite these advances, many open questions remain. Reasonably complete models are very hard to solve analytically, so it remains to be seen what extensions of the results for simple models are possible. Given the increasing parallels with problems in communication and finance, there is large scope for collaborations with specialists in those areas. The tools reviewed here are necessary because for it to be approachable by interdisciplinary collaborations, a formal description of the problem is needed. Since the analytical results presented here give clear predictions but for limited situations, those cases need to be tested experimentally to ensure any further advances rest on a solid foundation. In particular, we propose to expose populations to changing media in different runs where instead of the (average) period the transition probabilities are changed, over a timescale of hundreds of generations. If done for a well characterized

system like the lac operon, this would allow for a direct test of the adaptive changes in  $\hat{\pi}(g|c)$ .

A longer term goal could be the incorporation of information as a standard quantity alongside mass and energy in optimization arguments in other fields such as behavioral ecology. While much work would need to be done in solidifying and expanding the results mentioned here before they can be used across fields, it could be extremely fruitful. Some of the most powerful types of findings in physical systems are conserved quantities, as they provide the basic limitations to any dynamical process. Should information flow solidify into a similar rule in biology, it could greatly expand the

number of cases where an optimization procedure can be used predictively.

## AUTHOR CONTRIBUTIONS

JP wrote the article, and all authors conducted background research and edited the final version.

## FUNDING

This work was partially funded by the Faculty of Science at Universidad de los Andes.

## REFERENCES

- Quastler H. *Essays on the Use of Information Theory in Biology*. Urbana: University of Illinois Press (1953).
- Yang Z, Bielawski JP. Statistical methods for detecting molecular adaptation. *Trends Ecol Evol.* (2000) 15:496–503. doi: 10.1016/S0169-5347(00)01994-7
- Reiss MJ. Optimization theory in behavioural ecology. *J Biol Educ.* (1987) 21:241–7. doi: 10.1080/00219266.1987.9654909
- Shannon CE. A mathematical theory of communication. *Bell Syst Tech J.* (1948) 27:379–423. doi: 10.1002/j.1538-7305.1948.tb01338.x
- Howard R. Information value theory. *IEEE Trans. Syst. Sci. Cybern.* (1966) SSC-2:22–6. doi: 10.1109/TSSC.1966.300074
- Toprak E, Veres A, Yildiz S, Pedraza JM, Chait R, Paulsson J, et al. Building a morbidostat: an automated continuous-culture device for studying bacterial drug resistance under dynamically sustained drug inhibition. *Nat Protoc.* (2013) 8:555. doi: 10.1038/nprot.2013.021
- Shoresh N, Hegreness M, Kishony R. Evolution exacerbates the paradox of the plankton. *Proc Natl Acad Sci USA.* (2008) 105:12365–9. doi: 10.1073/pnas.0803032105
- Gardner TS, Cantor CR, Collins JJ. Construction of a genetic toggle switch in *Escherichia coli*. *Nature* (2000) 403:339–42. doi: 10.1038/35002131
- Lenski RE, Travisano M. Dynamics of adaptation and diversification: a 10,000-generation experiment with bacterial populations. *Proc Natl Acad Sci USA.* (1994) 91:6808–14. doi: 10.1073/pnas.91.15.6808
- Cohen D. Optimizing reproduction in a randomly varying environment. *J Theor Biol.* (1966) 12:119–29. doi: 10.1016/0022-5193(66)90188-3
- Thattai M, van Oudenaarden A. Stochastic gene expression in fluctuating environments. *Genetics* (2004) 167:523–30. doi: 10.1534/genetics.167.1.523
- Slatkin M. Hedging one's evolutionary bets. *Nature* (1974) 250:704.
- Avlund M, Dodd IB, Semsey S, Sneppen K, Krishna S. Why do phage play dice? *J Virol.* (2009) 83:11416–20. doi: 10.1128/JVI.01057-09
- Acar M, Mettetal JT, van Oudenaarden A. Stochastic switching as a survival strategy in fluctuating environments. *Nat Genet.* (2008) 40:471–5. doi: 10.1038/ng.110
- Paulsson J. Summing up the noise in gene networks. *Nature* (2004) 427:415. doi: 10.1038/nature02257
- Fraser HB, Hirsh AE, Giaever G, Kumm J, Eisen MB. Noise minimization in eukaryotic gene expression. *PLoS Biol.* (2004) 2:e137. doi: 10.1371/journal.pbio.0020137
- Raser JM, O'Shea EK. Noise in gene expression: origins, consequences, and control. *Science* (2005) 309:2010–3. doi: 10.1126/science.1105891
- Blake WJ, Balázsi G, Kohanski MA, Isaacs FJ, Murphy KE, Kuang Y, et al. Phenotypic consequences of promoter-mediated transcriptional noise. *Mol Cell* (2006) 24:853–65. doi: 10.1016/j.molcel.2006.11.003
- Lewis K. Persister cells. *Annu Rev Microbiol.* (2010) 64:357–72. doi: 10.1146/annurev.micro.112408.134306
- Balaban NQ, Merrin J, Chait R, Kowalik L, Leibler S. Bacterial persistence as a phenotypic switch. *Science* (2004) 305:1622–5. doi: 10.1126/science.1099390
- Maynard-Smith J. Optimization theory in evolution. *Annu Rev Ecol Syst.* (1978) 9:31–56. doi: 10.1146/annurev.es.09.110178.000335
- Gould SJ, Lewontin RC. The Spandrels of San Marco and the panglossian paradigm: a critique of the adaptationist programme. *Proc R Soc Lond B Biol Sci.* (1979) 205:581–98. doi: 10.1098/rspb.1979.0086
- Maynard-Smith J. The concept of information in biology. *Philos Sci.* (2000) 67:177–94. doi: 10.1086/392768
- Cerullo MA. The problem with phi: a critique of integrated information theory. *PLoS Comput Biol.* (2015) 11:e1004286. doi: 10.1371/journal.pcbi.1004286
- Sarkar S, editor. Biological information: a skeptical look at some central dogmas of molecular biology. In: *The Philosophy and History of Molecular Biology*. Dordrecht: Kluwer Academic Publishers (1996). p. 187–231.
- Gadiraju S, Vihlidal CA, Leeder JS, Rogan PK. Genome-wide prediction, display and refinement of binding sites with information theory-based models. *BMC Bioinformatics* (2003) 4:38. doi: 10.1186/1471-2105-4-38
- Rieke F, Warland D, Deruyter-van Steveninck R, Bialek W. *Spikes : Exploring the Neural Code*. The MIT Press (1999).
- Schneider TD, Stormo GD, Gold L, Ehrenfeucht A. Information content of binding sites on nucleotide sequences. *J Mol Biol.* (1986) 188:415–31. doi: 10.1016/0022-2836(86)90165-8
- Savir Y, Kagan J, Tlusty T. Binding of transcription factors adapts to resolve information-energy tradeoff. *J Stat Phys.* (2016) 162:1383–94. doi: 10.1007/s10955\_015-1388-5
- Seoane LF, Solé RV. Information theory, predictability and the emergence of complex life. *R Soc Open Sci.* (2018) 5:172221. doi: 10.1098/rsos.172221
- Adami C. The use of information theory in evolutionary biology. *Ann N Y Acad Sci.* (2012) 1256:49–65. doi: 10.1111/j.1749-6632.2011.06422.x
- Dimitrov AG, Lazar AA, Victor JD. Information theory in neuroscience. *J Comput Neurosci.* (2011) 30:1–5. doi: 10.1007/s10827-011-0314-3
- Massey JL. Causality, feedback, and directed information. In: *Proceedings IEEE International Symposium on Information Theory*. Honolulu, HI (1990). p. 303–5.
- Fisher RA. On the mathematical foundations of theoretical statistics. *Phil Trans R Soc Lond A* (1922) 222:309–68. doi: 10.1098/rsta.1922.0009
- Kinney JB, Atwal GS. Equitability, mutual information, and the maximal information coefficient. *Proc Natl Acad Sci USA.* (2014) 111:3354–9. doi: 10.1073/pnas.1309933111
- Day EK, Sosale NG, Lazzara MJ. Cell signaling regulation by protein phosphorylation: a multivariate, heterogeneous, and context-dependent process. *Curr Opin Biotechnol.* (2016) 40:185–92. doi: 10.1016/j.copbio.2016.06.005
- Farkash-Amar S, Zimmer A, Eden E, Cohen A, Geva-Zatorsky N, Cohen L, et al. Noise genetics: inferring protein function by correlating phenotype with protein levels and localization in individual human cells. *PLoS Genet.* (2014) 10:e1004176. doi: 10.1371/journal.pgen.1004176
- Massicot R, Whitelaw E, Angers B. DNA methylation: a source of random variation in natural populations. *Epigenetics* (2011) 6:421–7. doi: 10.4161/epi.6.4.14532

## Origin of Reproducibility in the Responses of Retinal Rods to Single Photons

F. Rieke\*# and D. A. Baylor\*

\*Department of Physiology and Biophysics, University of Washington, Seattle, Washington 98195 and #Department of Neurobiology, Stanford University, Stanford, California 94305 USA

**ABSTRACT** The single photon responses of retinal rod cells are remarkably reproducible, allowing the number and timing of photon absorptions to be encoded accurately. This reproducibility is surprising because the elementary response arises from a single rhodopsin molecule, and typically signals from single molecules display large intertrial variations. We have investigated the mechanisms that make the rod's elementary response reproducible. Our experiments indicate that reproducibility cannot be explained by saturation within the transduction cascade, by  $\text{Ca}^{2+}$  feedback, or by feedback control of rhodopsin shutoff by any known element of the cascade. We suggest instead that deactivation through a series of previously unidentified transitions allows the catalytic activity of a single rhodopsin molecule to decay with low variability. Two observations are consistent with this view. First, the time course of rhodopsin's catalytic activity could not be accounted for by the time required for the known steps in rhodopsin deactivation—phosphorylation and arrestin binding. Second, the variability of the elementary response increased when phosphorylation was made rate-limiting for rhodopsin shutoff.

### INTRODUCTION

This work examines the mechanism that enables retinal rod cells to register single photon absorptions with macroscopic signals of constant size and shape. Constancy of the elementary response is essential if the number and timing of photon absorptions are to be accurately represented. The classic frequency of seeing experiments of Hecht et al. (1942) and van der Velden (1946) established that the human visual system can detect the absorption of a few photons and that individual rods can successfully detect single photons. More recent work by Sakitt (1972) suggests that the visual system can literally count photon absorptions beginning at one or two, requiring the rods to encode accurate information about the number of absorbed photons. Photon counting would not be possible if the rod's elementary response fluctuated widely, as small responses would not be sensed by central neurons and large responses would mimic the effect of multiple photon absorptions. Variations in the shape of the elementary response would also degrade information about the timing of photon absorption and thus impair the temporal precision of rod vision. As photon absorptions occur rarely in each rod over much of the intensity range of rod vision, accurate registration of the number and timing of photon absorptions is important for normal rod vision.

It is well known that reliable photon detection requires amplification and low dark noise. The amplification is achieved by the cascade diagrammed in Fig. 1 (reviewed by Pugh and Lamb, 1993). An effective photon absorption photoisomerizes a rhodopsin molecule, which becomes cat-

alytically active. A photoisomerized rhodopsin activates thousands of copies of the G-protein transducin (T), each of which can activate a catalytic subunit of phosphodiesterase (PDE). An activated PDE subunit typically hydrolyzes at least 50 cyclic guanosine monophosphate (cGMP) molecules (Pugh and Lamb, 1993; Rieke and Baylor, 1996). The resulting reduction in the cGMP concentration allows hundreds of cationic channels in the surface membrane to close, preventing more than  $10^6$  cations from entering the outer segment. This macroscopic decrease in inward current hyperpolarizes the cell membrane and slows transmitter release from the synaptic terminal. Dark noise in the transduction current arises primarily from thermal isomerization of rhodopsin and from spontaneous activation of PDE (Baylor et al., 1980; Rieke and Baylor, 1996). Although the dark noise is relatively low, it appears to limit the absolute sensitivity of vision (Aho et al., 1988).

The first evidence for the reproducibility of the rod's elementary electrical response came from statistical analysis of the photocurrents evoked by dim flashes (Baylor et al., 1979b, 1984), which revealed that the standard deviation of the response amplitude was only  $\sim 20\%$  of the mean and that the time course was nearly fixed. The molecular mechanism of this reproducibility is intriguing because the signals generated by many types of single particles show large intertrial fluctuations. Familiar examples are the amount of charge transferred during an ion channel's open time and the time required for the decay of a radioactive atom. Such fluctuations arise from stochastic variations in the active lifetime of the particle. The rod's elementary response should reflect variability in the timing of rhodopsin deactivation because rhodopsin drives the amplifying cascade while it remains active. Yet the fluctuations in the elementary response are remarkably small. This might be explained in either of two ways: 1) the elementary response might be insensitive to variations in rhodopsin's active lifetime, or 2)

widely,  
amplamente  
inward,  
interior

Received 26 March 1998 and in final form 7 July 1998.  
Address reprint requests to Dr. Fred Rieke, Department of Physiology and Biophysics, University of Washington, Seattle, WA 98195.  
Fax: 206-685-0619; E-mail: rieke@u.washington.edu.  
© 1998 Society for Neuroscience  
0270-6474/98/751836-12\$15.00/0

Shutoff - ciene

efflux - defljo<sup>r</sup>

efljo<sup>r</sup>

in flux - infljo<sup>r</sup>

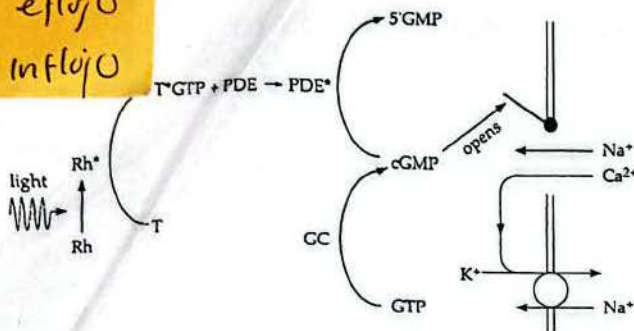


**FIGURE 1** Diagram of phototransduction cascade. Effective absorption of a photon activates the photopigment rhodopsin (Rh); the cascade amplifies rhodopsin's activity to create a macroscopic electrical response. Active rhodopsin catalyzes the activation of the G protein transducin (T), which in turn activates phosphodiesterase (PDE). Activated PDE hydrolyzes cGMP, causing its concentration to fall, channels in the surface membrane to close, and the current flowing into the outer segment to decrease. The cGMP concentration and dark current are restored by cGMP synthesis by guanylate cyclase (GC). The recovery of the flash response is accelerated by Ca<sup>2+</sup> feedback. Ca<sup>2+</sup> enters the cell through the cGMP-gated channels and is extruded by Na<sup>+</sup>/K<sup>+</sup>, Ca<sup>2+</sup> exchange. Influx of Ca<sup>2+</sup> slows during the light response while efflux continues, causing the internal Ca<sup>2+</sup> concentration to drop. The fall in Ca<sup>2+</sup> concentration increases the rate of cGMP synthesis and thus speeds the return of the cGMP concentration and current to their respective dark values.

the active lifetime might have low variability. We present evidence favoring the second possibility and explore the contributions of several mechanisms.

## MATERIALS AND METHODS

The experiments were carried out on isolated rods from the dark-adapted retina of the toad *Bufo marinus*, as described by Rieke and Baylor (1996). Single rods were isolated by shredding a small piece of retina, and their membrane current was recorded with a suction electrode (Baylor et al., 1979a). Experiments were performed on intact cells or on truncated, internally dialyzed outer segments. In either case, membrane current collected by the suction electrode was amplified, low-pass filtered at 20 Hz (-3 dB point; 8-pole Bessel low-pass), and digitized at 100 Hz. Light responses were elicited by 10-ms flashes of 500-nm light; the flash strength was controlled with calibrated neutral density filters. The cell was usually positioned in the suction electrode to collect as much dark current as possible. In some experiments the contribution of cellular dark noise to the measured current was minimized by drawing only the tip of the outer segment into the suction electrode and applying the stimulating flash as a transverse slit 10  $\mu\text{m}$  wide. The transverse slit was also used in experiments on truncated outer segments because the shape of the response depended on the longitudinal distance from the site of truncation; in these experiments the center of the slit was positioned ~20  $\mu\text{m}$  from the cut end of the outer segment. In all experiments a half-saturating response was measured periodically to check the stability of the cell, and the experiment was terminated if the response changed significantly.

Table 1 gives the compositions of the solutions. Solution changes were usually achieved with a series of electronically controlled pinch valves (Biochem Valves, Boonton, NJ) whose outlets were connected to a common perfusion pipe ~100  $\mu\text{m}$  in diameter. Solution changes with this system were completed in 200–300 ms, as judged by junction potential measurements. In measurements of rhodopsin's catalytic activity (Fig. 7), faster solution changes were achieved by moving the interface between two continuously flowing solutions across the outer segment. Solutions were driven by positive pressure through a pair of glass pipes with openings ~50

## Reproducibility of the Single Photon Response

**TABLE 1** Solutions

	HEPES Ringer's	Bicarbonate Ringer's	Truncation dialysis	Truncation electrode	Ca <sup>2+</sup> clamp
NaCl (mM)	120	87	—	120	—
KCl	2	2	—	—	—
NaHCO <sub>3</sub>	2	35	—	—	—
CaCl <sub>2</sub>	1	1	0.75	0.05	0.25
MgCl <sub>2</sub>	1.6	1.6	1.6	1.6	—
Glucose	10	10	—	—	—
Hepes	3	3	3	3	3
EGTA	—	—	1	—	—
BAPTA	—	—	—	—	—
Arginine- glutamate	—	—	120	—	—
Choline-Cl	—	—	—	—	120

Compositions of each solution. The pH was adjusted to 7.6 with TMA-OH in the truncation internal and Ca<sup>2+</sup> clamp solutions and with Na-OH in the other solutions. The osmolarity was 245 in the truncation dialysis solution and 260 in all others. The free Ca<sup>2+</sup> concentration in the truncation dialysis solution was 500–600 nM unless otherwise noted.

$\mu\text{m}$  in diameter; the pipes were mounted on a piezoelectric translation stage (Burleigh Instruments, Fishers, NY). Solution changes at the cut end of the outer segment were completed in less than 10 ms with this system.

One set of experiments (those of Fig. 16) required a complete change of the nucleotide concentrations within the outer segment during the flash response. This was difficult at room temperature, as the time required for diffusion into the outer segment was comparable to the duration of the flash response. At 5–8°C, however, the duration of the flash response was much longer than the diffusion time. Low temperatures were achieved by cooling the solutions entering the chamber with a Peltier device (Ferrotec America, Chelmsford, MA) and blowing cold, dry air from a vortex tube (Illinois Tool Works, Glenview, IL) over the chamber. The temperature near the outer segment was monitored with a small thermocouple (Harvard Apparatus, Holliston, MA). All solutions flowed continuously to ensure that the temperature was uniform and steady; solution changes were made with the pipes mounted on the piezoelectric translation stage as described above.

In some experiments changes in the outer segment's free internal Ca<sup>2+</sup> concentration were suppressed by inhibiting Ca<sup>2+</sup> influx and efflux. Ca<sup>2+</sup> efflux was inhibited by removing internal K<sup>+</sup> or external Na<sup>+</sup>, both of which are required for Na<sup>+</sup>/K<sup>+</sup>, Ca<sup>2+</sup> exchange (Cervetto et al., 1989); Ca<sup>2+</sup> influx was inhibited by lowering the external Ca<sup>2+</sup> concentration to reduce or eliminate the driving force on Ca<sup>2+</sup> ions. For truncated outer segments (Yau and Nakatani, 1985), K<sup>+</sup> was omitted from the dialyzing solution and the solution in the suction electrode; the free Ca<sup>2+</sup> concentration was buffered to 500–600 nM in the dialyzing solution and to a few nM inside the suction electrode. For intact cells, the inner segment was held in the suction electrode while the outer segment was superfused with a solution lacking Na<sup>+</sup> and Mg<sup>2+</sup> and containing 10–20 nM free Ca<sup>2+</sup> (Nakatani and Yau, 1988a; Matthews et al., 1988). Under these conditions the dark current was carried by outward movement of K<sup>+</sup> and remained relatively stable (<10% change) for periods of 30–60 s, after which the outer segment was superfused with Ringer's for at least 30 s.

The experiment illustrated in Fig. 2 tested for residual light-induced changes in the free Ca<sup>2+</sup> concentration in intact cells whose outer segments were superfused with a solution lacking Na<sup>+</sup> and containing low Ca<sup>2+</sup>. Dim flash responses were recorded from an intact rod with the Ca<sup>2+</sup> changing freely (thin trace in Fig. 2A) or with changes in Ca<sup>2+</sup> suppressed (thin trace in Fig. 2B). The rod was then superfused for 15 min with a solution containing 10  $\mu\text{M}$  BAPTA-AM, a membrane-permeable Ca<sup>2+</sup>-buffer. Responses to the flash were recorded again with the Ca<sup>2+</sup> changing freely or held constant (thick traces in Fig. 2, A and B). Increasing the Ca<sup>2+</sup> buffering capacity of the outer segment should slow changes in free Ca<sup>2+</sup> and thus render Ca<sup>2+</sup> feedback less effective in accelerating the flash response. Indeed, exposure to BAPTA slowed the control flash response

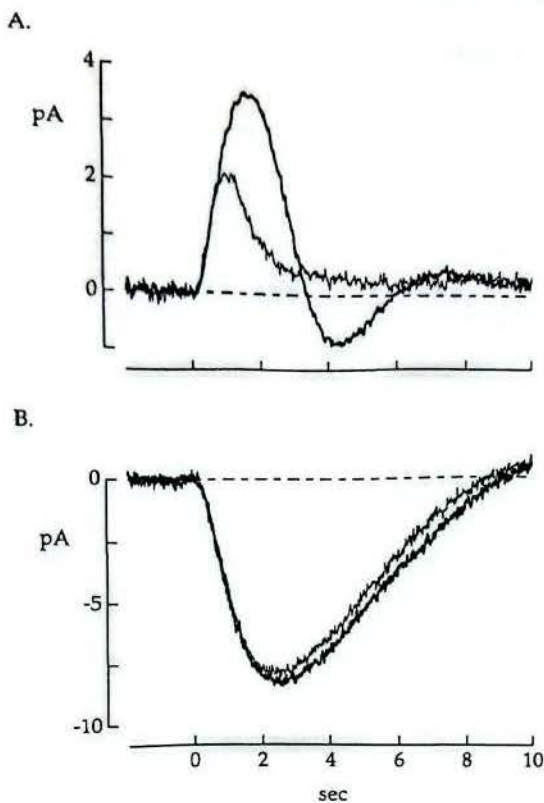


**FIGURE 2** Test for residual light-induced changes in the internal  $\text{Ca}^{2+}$  concentration when the outer segment was superfused with a  $0 \text{ Na}^+$ , low  $\text{Ca}^{2+}$  solution (see Materials and Methods). Flash strength was  $1.3 \text{ photons } \mu\text{m}^{-2}$ . (A) Dim flash responses measured in an intact rod with the inner segment in the suction electrode and the outer segment superfused with Ringer's, allowing the  $\text{Ca}^{2+}$  concentration to change freely. The response shown by the thin trace was measured before exposure to BAPTA-AM; the response shown by the thick trace was measured after the cell was superfused with  $10 \mu\text{M}$  BAPTA-AM for 15 min and returned to Ringer's. Increasing the  $\text{Ca}^{2+}$  buffering capacity of the outer segment by exposure to BAPTA-AM clearly altered the dim flash response. The dark current with the  $\text{Ca}^{2+}$  changing freely was  $-13 \text{ pA}$ . (B) Dim flash responses measured from the same cell as in A, but with light-induced changes in the internal  $\text{Ca}^{2+}$  concentration suppressed by superfusing the outer segment with a solution lacking  $\text{Na}^+$  and containing low  $\text{Ca}^{2+}$ . The response shown by the thin trace was measured before BAPTA exposure, the response shown by the thick trace after. The addition of  $\text{Ca}^{2+}$  buffer to the outer segment had only a small effect on the dim flash response, indicating that residual light-induced changes in  $\text{Ca}^{2+}$  were small on the time scale of the response. The dark current was  $+16 \text{ pA}$ .

and made it biphasic (Fig. 2A), as observed previously (Torre et al., 1986). If changes in the internal  $\text{Ca}^{2+}$  alter the flash response when the outer segment is superfused with the  $0 \text{ Na}^+$ , low  $\text{Ca}^{2+}$  solution, the addition of BAPTA would alter the flash response under these conditions as well. In this case, however, the flash response changed little (Fig. 2B). In three experiments of this type, changes in the time to peak and amplitude after the addition of BAPTA were at least fivefold smaller with the  $\text{Ca}^{2+}$  held constant than with it changing freely. The relative insensitivity of the flash response to exogenous buffer indicates that superfusion with the  $0 \text{ Na}^+$ , low  $\text{Ca}^{2+}$  solution effectively suppressed light-induced changes in  $\text{Ca}^{2+}$  within the outer segment.

## THEORY

This section presents a model that relates the statistics of rhodopsin shutoff to the time-dependent mean and variance

of the elementary response. We use this model in two ways. In the Results, the calculated mean and variance are compared to the quantities measured when rhodopsin shutoff was slowed and presumably made more variable (see Figs. 12 and 17). In the Discussion, the model is used to explore how the low variability of the elementary response constrains possible mechanisms of reproducibility (Fig. 18). The parameters of the model were held fixed for all calculations, as the aim was to explore classes of models for reproducibility rather than to provide accurate fits to individual measurements.

### Relation between rhodopsin activity and change in current

We begin by relating the time course of rhodopsin's catalytic activity to changes in PDE activity, cGMP concentration, and membrane current. The model for the transduction cascade is similar to that of Pugh and Lamb (1993) and Nikonov et al. (1998). A more complete description can be found in Rieke and Baylor (1996).

Active rhodopsin decreases the cGMP concentration by catalyzing the activation of transducin, which in turn activates a cGMP phosphodiesterase (PDE) (Fig. 1). As this latter step occurs quickly (reviewed by Pugh and Lamb, 1993), we ignore any delay introduced by transducin activation and approximate the time derivative of the PDE activity  $P(t)$  as

$$\frac{dP(t)}{dt} = \sigma R(t) - \phi(P(t) - P_D), \quad (1)$$

where  $\sigma R$  is the rate of PDE activation for a rhodopsin activity  $R$ ,  $\phi$  is the rate constant for PDE deactivation, and  $P_D$  is the dark PDE activity. Equation 1 describes the light-induced change in PDE activity as the output of a low-pass filter with time constant  $\phi^{-1}$  applied to rhodopsin's catalytic activity.

The time derivative of the cGMP concentration  $G(t)$  depends on the difference between the rates of cGMP synthesis and hydrolysis (Fig. 1),

$$\frac{dG(t)}{dt} = \gamma - P(t)G(t), \quad (2)$$

where  $\gamma$  is the rate of cGMP synthesis. Pugh and Lamb (1993) applied Eq. 2 at short times after a flash, assuming that the synthesis rate was constant, that the PDE activity could be approximated by a delayed ramp, and that  $P(t) \gg P_D$ . In this case the change in cGMP concentration is proportional to  $\exp(-at^2)$ , where  $a$  is a constant proportional to the flash strength. Their analysis accurately describes the initial rise of the flash response.

In intact rods, a light-induced fall in the free  $\text{Ca}^{2+}$  concentration affects several elements of the transduction cascade (reviewed by Koutalos and Yau, 1996). The most pronounced of these effects is an increase in the rate of cGMP synthesis and a consequent speeding of response

recovery, and for simplicity we will include only this effect of  $\text{Ca}^{2+}$  in the model. The free  $\text{Ca}^{2+}$  concentration depends on the rates of  $\text{Ca}^{2+}$  influx through the cGMP-gated channels and  $\text{Ca}^{2+}$  efflux by  $\text{Na}^+/\text{K}^+$ ,  $\text{Ca}^{2+}$  exchange (Nakatani and Yau, 1988b; Cervetto et al., 1989). Although a complete description of the exchange rate requires several time constants (Rispoli et al., 1993; Gray-Keller and Detwiler, 1994; McCarthy et al., 1996; Murnick and Lamb, 1996), the fastest component should dominate during the flash response. Thus the time derivative of the free  $\text{Ca}^{2+}$  concentration  $C$  can be approximated by

$$\frac{dC(t)}{dt} = qI(t) - \beta C(t), \quad (3)$$

where  $q$  is a constant relating changes in the free  $\text{Ca}^{2+}$  concentration to the membrane current  $I$  (Nakatani and Yau, 1988b), and  $\beta$  is the rate constant for  $\text{Ca}^{2+}$  efflux.  $\beta$  depends on the activity of both the exchange proteins and intracellular  $\text{Ca}^{2+}$  buffers. The dependence of the rate of cGMP synthesis on the free  $\text{Ca}^{2+}$  concentration can be described by the Hill curve (Koch and Stryer, 1988; Koutalos et al., 1995a):

$$\gamma = \frac{\gamma_{\max}}{1 + (C/K_{GC})^m} \approx \frac{\gamma_{\max} K_{GC}^m}{C^m}, \quad (4)$$

where  $\gamma_{\max}$  is the maximum synthesis rate,  $K_{GC}$  and  $m$  are affinity and cooperativity constants, and the approximation is valid for  $C \gg K_{GC}$ . This approximation should hold for small changes in the current, as the free  $\text{Ca}^{2+}$  concentration in darkness is two to three times greater than  $K_{GC}$ .

We write the change in cGMP concentration as  $g(t) = G(t) - G_D$ , where  $G_D$  is the dark cGMP concentration.  $g(t)$  can be approximated from Eqs. 1–5 as a filtered version of the rhodopsin activity  $R(t)$ , assuming that the changes in the PDE activity, cGMP concentration, and free  $\text{Ca}^{2+}$  concentration are small relative to the dark values (see Rieke and Baylor, 1996):

$$g(t) \approx \int_0^t F(\tau)R(t-\tau)d\tau. \quad (5)$$

When the free  $\text{Ca}^{2+}$  concentration and hence the synthesis rate  $\gamma$  are constant, the Fourier transform of the filter  $F$  is given by

$$\tilde{F}(\omega) = -\frac{\sigma G_D}{(\phi - i\omega)(P_D - i\omega)}, \quad (6)$$

where  $\omega = 2\pi f$  is the angular frequency in radians per second and  $\tilde{F}(\omega) = \int_{-\infty}^{\infty} \exp(i\omega t)F(t)dt$ . When the  $\text{Ca}^{2+}$  concentration changes freely, the Fourier transform of the filter

takes the form

$$\tilde{F}(\omega) = -\frac{\sigma G_D}{(\phi - i\omega)} \left[ P_D + \frac{3m\beta^2 P_D}{\beta^2 + \omega^2} - i\omega + \frac{3mi\omega\beta P_D}{\beta^2 + \omega^2} \right]^{-1}. \quad (7)$$

The changes in cGMP concentration described by Eqs. 5–7 depend on two time scales: 1) that for the decay of the light-activated PDE activity, determined by the time course of rhodopsin's catalytic activity and the decay rate  $\phi$  of PDE; and 2) that for the restoration of the cGMP concentration, determined by the dark cGMP synthesis rate (equal to  $P_D G_D$ ) and the rate constant  $\beta$  for the fall in  $\text{Ca}^{2+}$ . For all calculations we assumed  $m = 2$ ,  $P_D = 0.1 \text{ s}^{-1}$ ,  $\phi = 2 \text{ s}^{-1}$ , and  $\beta = 2 \text{ s}^{-1}$  (see Koutalos et al., 1995a,b; Rieke and Baylor, 1996).

Equation 5 describes the change in the internal cGMP concentration produced by rhodopsin activity. The membrane current rapidly tracks this change (Karpen et al., 1988), and for cGMP concentrations at which less than half the channels are open, the current can be approximated as (Zimmerman and Baylor, 1986)

$$I \approx kG^3, \quad (8)$$

where  $k \approx 8 \times 10^{-3} \text{ pA}/\mu\text{M}^3$  in toad rods (Rieke and Baylor, 1996). The approximation in Eq. 8 should be valid for the experiments described here; in intact cells  $\sim 5\%$  of the channels were open in the dark, whereas in experiments on truncated outer segments 10–20% of the channels were open in darkness. Assuming  $g(t) \ll G_D$ , Eq. 8 can be expanded and approximated by the linear term. The result is that the change in current  $i(t)$  is approximately

$$i(t) = I_D - I(t) \approx -3kG_D^2 g(t). \quad (9)$$

Equation 9 should provide a good description of the single photon current response, as the change in cGMP is thought to be small compared to the dark value at all points along the outer segment (Pugh and Lamb, 1993). Equations 5 and 9 can be combined to estimate the current change produced by rhodopsin activity  $R(t)$ ,

$$i(t) \approx -3kG_D^2 \int_0^t F(\tau)R(t-\tau)d\tau, \quad (10)$$

where the Fourier transform of the filter  $F(\tau)$  is given by Eq. 6 or 7.

The model described above treats the cGMP and  $\text{Ca}^{2+}$  concentrations as spatially homogeneous, ignoring diffusion. If the current change in an intact rod is linearly related to rhodopsin activity, then the time course and amplitude of the current response depend only on the total changes in cGMP and  $\text{Ca}^{2+}$  and not on their spatial extent. In this case diffusion can be ignored. In truncated outer segments, diffusion causes the cGMP concentration to depend on longitudinal position, and in outer segments without cGMP syn-

thesis, diffusion restores the cGMP concentration and dark current. To test the effect of diffusion on the single photon response in truncated outer segments with cGMP synthesis proceeding normally, we compared the behavior of the model described above with that of a model including cGMP diffusion (see Rieke and Baylor, 1996). Calculated flash responses with and without diffusion were nearly identical, and thus for simplicity we neglected diffusion. Dim flash responses in truncated outer segments without cGMP synthesis were fitted assuming that restoration of the cGMP concentration by diffusion occurred at a constant rate  $\gamma_{\text{eff}}$ . This simplified treatment again provided calculated responses in close agreement with those calculated when diffusion was included.

### Stochastic model for rhodopsin shutoff

Equation 10 provides an estimate of the elementary current response given the time course of the activity of a single photoisomerized rhodopsin molecule. Intertrial fluctuations in the response could arise either from variations in the time course of rhodopsin's activity or from fluctuations in the transduction cascade. Because a single active rhodopsin rapidly generates hundreds or thousands of active transducin molecules (reviewed by Pugh and Lamb, 1993), stochastic fluctuations in the transducin activity or transducin's activation products should be small compared to fluctuations in the rhodopsin activity. In this case the filter  $F$  is effectively deterministic, and variability in the elementary response can be attributed to rhodopsin. To investigate how the measured response fluctuations constrain fluctuations in the rhodopsin activity, we considered two stochastic models for rhodopsin shutoff. In each model the time course of the catalytic activity of a single rhodopsin molecule was calculated and the corresponding elementary response was generated from Eq. 10, which assumes that the cascade responds linearly and deterministically to rhodopsin activity. This procedure was repeated for several hundred trials, and the time-dependent ensemble mean and variance were calculated and compared with experiment (Fig. 18).

The effect of feedback control of rhodopsin shutoff on the mean and variance of the elementary response was investigated assuming that the putative feedback signal accumulated linearly with time and accelerated rhodopsin shutoff with a cooperativity  $h$ . Thus the feedback caused the probability density for rhodopsin shutoff to increase proportionally with  $t^h$ , where  $t$  is the time after photoisomerization. Shutoff was assumed to occur as a single step.

The effect of multiple transitions in rhodopsin shutoff on the mean and variance of the elementary response was investigated assuming that each transition was memoryless and first-order. Transitions were assumed to occur sequentially with rate constants proportional to the catalytic activity of the state preceding the transition; thus states with low catalytic activity decayed more slowly than states with high activity. This choice of rate constants and activities was

made for two reasons. First, this model distributes rhodopsin's cumulative activity equally among the states and produces the maximum reduction in the variance of the elementary response for a given number of states. Second, a gradual decline in rhodopsin activity is consistent with the approximately exponential time course of rhodopsin's activity measured in Fig. 7.

## RESULTS

### Reproducibility of the single photon response

Variability in the amplitude and time course of the elementary response constrains the mechanisms responsible for reproducibility. Thus we analyzed the statistics of the responses to a fixed dim flash, producing an average of less than one photoisomerization per trial; a short section of one such experiment is shown in Fig. 3 A. Each flash generated zero, one, or two photoisomerizations and a quantized change in current. The intertrial variability in the response is consistent with the Poisson statistics that govern the probability of photoisomerization (Baylor et al., 1979b; see below). Each elementary response had a similar amplitude and shape. This reproducibility allows responses to zero, one, or two photoisomerizations to be clearly distinguished, as shown in Fig. 3 B, where 50 individual responses are superimposed. The largest response presumably resulted from two or three photoisomerizations. Thus the rod is an accurate photon counter that reliably detects a single photoisomerization and differentiates between one and two photoisomerizations.

### Variability of the response amplitude and time course

The accuracy with which the number and timing of photoisomerizations can be deduced from the rod current is limited by cellular dark noise and variability in the elementary response. We investigated the fluctuations in the elementary response itself by separating them from dark noise, which consists of continuous baseline fluctuations and occasional discrete events caused by the thermal activation of rhodopsin (Baylor et al., 1980). Discrete events were identified as those occurring at times unrelated to the flash (arrows in Fig. 3 A); trials containing a discrete event were removed before the statistics of the remaining responses were analyzed. Elementary response fluctuations were separated from continuous dark noise by comparing responses to zero and one photoisomerization, as described below.

Fig. 4 A shows a histogram of the response amplitudes, measured as the difference between the mean current in a 0.5 s interval before the flash and a similar interval centered on the maximum of the average response (shown in inset). The peaks in the histogram correspond, respectively, to zero, one, and two photoisomerizations. Amplitude histograms were fitted assuming that responses to individual photoisomerizations were additive, that the number of photoisomerizations produced by repeated flashes obeyed Pois-

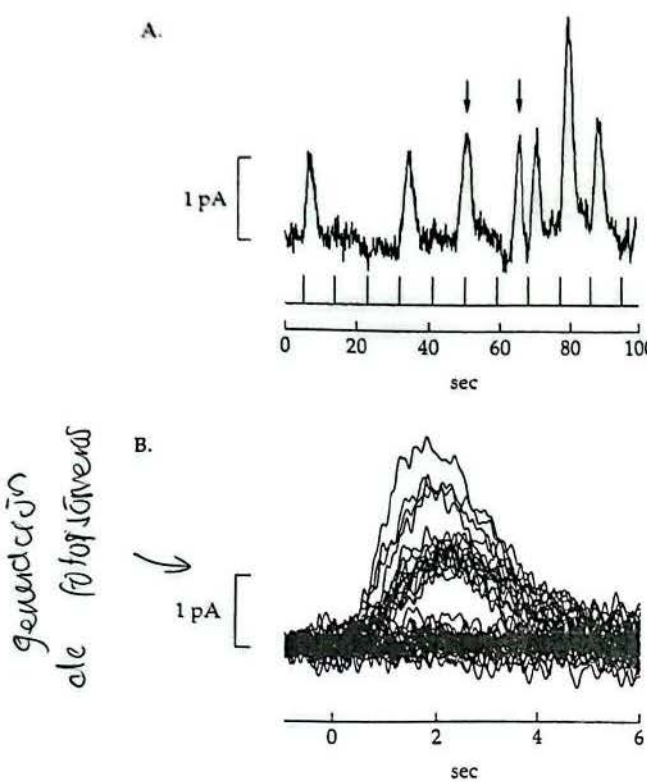


**FIGURE 3** Single photon responses. (A) Photocurrents from an intact rod stimulated by a series of dim flashes delivered at the times indicated by the flash monitor. The flashes produced an average of 0.7 photoisomerizations per trial. Two events from spontaneous rhodopsin isomerization are marked by arrows. The outer segment was in the suction electrode, and the cell was superfused with a bicarbonate-based Ringer's. Flash stimuli were applied over a transverse slit 10  $\mu\text{m}$  wide positioned near the middle of the outer segment. Bandwidth: 0–3 Hz. The dark current was –25 pA. (B) Superimposed responses to 50 flashes, including those in A. The responses were recorded sequentially, except for the removal of responses clearly contaminated by thermal events (such as those marked by arrows in A). The mean current in a 1 s interval before the flash has been set to zero in each case to correct for baseline drift and to facilitate comparison of the response shapes. Responses to zero, one, and two photoisomerizations can be clearly distinguished, as each elementary response had an amplitude and time course similar to those of the others. The largest response presumably resulted from two or three photoisomerizations.

son statistics, and that the noise in darkness and in the elementary response amplitude were independent and additive with Gaussian amplitude distributions. The expected number of responses with an amplitude between  $A$  and  $A + \Delta A$  is

$$N(A) = N_{\text{tot}} \Delta A \sum_{n=0}^{\infty} \frac{\exp(-\bar{n}) \bar{n}^n}{n!} [2\pi(\sigma_D^2 + \bar{n}\sigma_A^2)]^{-1/2} \times \exp\left(-\frac{(A - \bar{n}\hat{A})^2}{2(\sigma_D^2 + \bar{n}\sigma_A^2)}\right), \quad (11)$$

where  $N_{\text{tot}}$  is the total number of responses,  $\hat{A}$  is the mean amplitude of the elementary response,  $\bar{n}$  is the mean number of photoisomerizations per flash,  $\sigma_D^2$  is the variance of the

current amplitude in darkness, and  $\sigma_A^2$  is the variance in the elementary response amplitude. The first term in the sum is the probability that the flash produced  $n$  photoisomerizations, and the remaining terms give the probability that the response to  $n$  photoisomerizations had an amplitude  $A$ . The smooth curve in Fig. 4 A was drawn according to Eq. 11, with  $N_{\text{tot}} = 410$ ,  $\hat{A} = 0.66$  pA,  $\bar{n} = 0.67$ ,  $\sigma_D = 0.09$  pA, and  $\sigma_A = 0.14$  pA. The ratio of the mean amplitude  $\hat{A}$  to its standard deviation  $\sigma_A$  provides a measure of the reproducibility of the elementary response amplitude. In 13 cells  $\hat{A}/\sigma_A$  was  $4.6 \pm 0.9$  (mean  $\pm$  SD). In five additional cells,  $\sigma_A$  was less than  $\sigma_D$  and could not be accurately estimated; in each of these cells  $\hat{A}/\sigma_A$  was greater than 5. Thus the mean amplitude of the elementary response was about five times larger than its standard deviation, in agreement with previous measurements (Baylor et al., 1979b; Schnapf, 1983).

The entire shape of the elementary response was also nearly constant across trials, as revealed by the following analysis. Responses to single photoisomerizations ("singles") were separated from responses to zero ("failures") or multiple photoisomerizations. For example, in Fig. 4 A responses with amplitudes between 0.3 and 1.0 pA were taken as singles. Each of these responses was fitted by the equation for the impulse response of a cascade of  $m$  identical and independent first-order low-pass filters,

$$i_{\text{fit}}(t) = a(t/\tau)^{m-1} \exp(-t/\tau), \quad (12)$$

where  $a$  is a scaling factor for the response amplitude and  $\tau$  is the time constant of each filter. Fitting was done by choosing the values of  $a$  and  $\tau$  that minimized the mean square error between  $i_{\text{fit}}(t)$  and  $i(t)$  for each response  $i(t)$  while holding  $m$  fixed at 4. A histogram of the values of  $\tau$  for the cell of Fig. 4 A is shown in Fig. 4 B. The dark noise contributed little to the width of the distribution, as judged by adding a fixed elementary response to each failure (responses with amplitudes less than 0.3 pA in Fig. 4 A) and fitting the resulting ensemble as before. The smooth curve in Fig. 4 B is a Gaussian with a mean  $\bar{\tau} = 0.58$  s and standard deviation  $\sigma_\tau = 0.12$  s. The ratio  $\bar{\tau}/\sigma_\tau$  provides a measure of the reproducibility of the shape of the elementary response. In 11 cells  $\bar{\tau}/\sigma_\tau$  was  $4.8 \pm 1.0$  (mean  $\pm$  SD). Thus both the mean amplitude and temporal width of the elementary response were about five times larger than their respective standard deviations. This degree of constancy provides a constraint for evaluating possible mechanisms for reproducibility.

#### Time-dependent variance of the elementary response

The low variability of the elementary response was verified by comparing the time-dependent variance of responses to a fixed dim flash with the square of the mean response. If the elementary response has a stereotyped waveform  $f(t)$  and the average number of isomerizations per flash is  $\bar{n}$ , then the mean response is  $\bar{n}f(t)$  and the variance due to Poisson

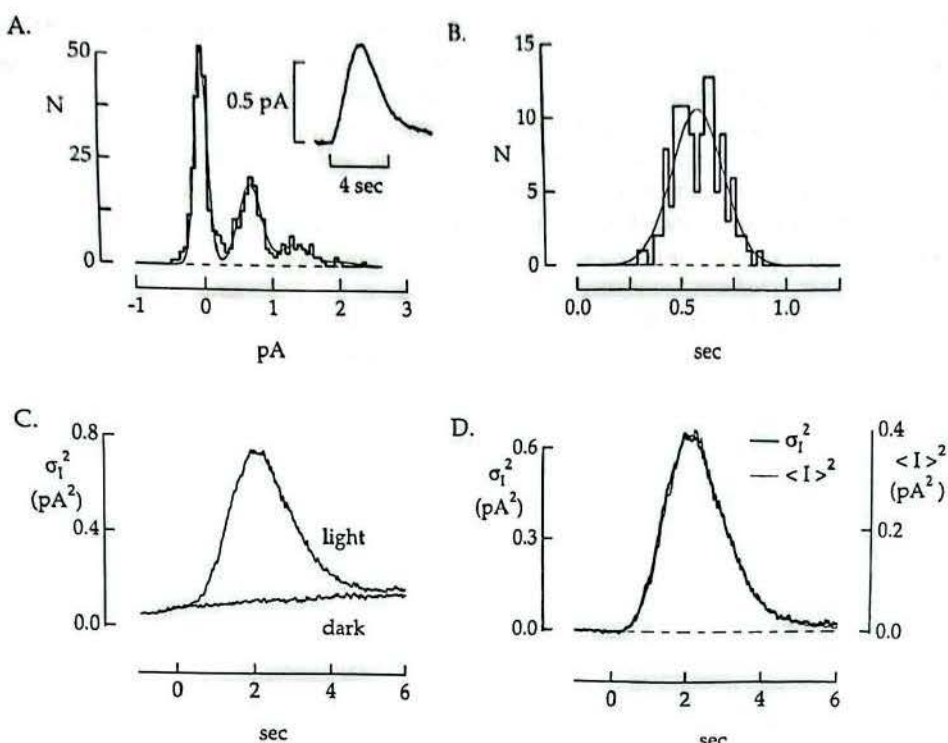


**FIGURE 4** Reproducibility of the single photon response. Recordings were made from an intact rod superfused with bicarbonate-based Ringer's with its outer segment in the suction electrode. Flash stimuli were applied over a transverse slit 10  $\mu m$  wide positioned near the middle of the outer segment. The dark current was  $-23$  pA. (A) Amplitude histogram constructed from a series of 410 dim flash responses like those in Fig. 3. The inset shows the mean response; the flash was delivered at the beginning of the horizontal scale bar. The amplitude of each response was measured as the average decrease in current between 1.75 and 2.25 s. The smooth curve fitted to the experimental histogram was calculated according to Eq. 11, which assumes that the noise in darkness and the noise in the elementary response amplitude are independent and additive and that the number of photoisomerizations per flash is described by Poisson statistics. The fit was calculated for 0.67 photoisomerizations per flash, a mean elementary response amplitude of 0.66 pA, a standard deviation of the current in darkness of 0.09 pA, and a standard deviation of the elementary response amplitude of 0.14 pA. (B) Histogram measuring reproducibility of the elementary response shape (stepped curve) constructed from the 129 responses from A, with an amplitude between 0.3 and 1.0 pA. Each response was fitted according to Eq. 12 with the output of a cascade of four identical, independent low-pass filters. The free variable in the fit was the low-pass filter time constant, and these time constants form the histogram plotted. The smooth curve is a Gaussian with a mean of 0.58 s and a standard deviation of 0.12 s. (C) Time-dependent variance of responses measured in darkness ("dark") and in the presence of the flash stimulus ("light"). The variance measured in darkness resulted from baseline drift and instrumental and cellular noise. The additional variance with light exposure arose from intertrial variability in the measured responses; this variance contains contributions from Poisson fluctuations in the number of photons absorbed per flash and variability in the elementary response. Same experiment as in A and B. (D) Light-dependent variance increase (thick trace) and square of the mean response (thin trace). The variance increase is the difference (light - dark) between the two traces in C. As described in the text, the variance increase would have the same shape as the square of the mean response if each photoisomerization produced an identical response and the variance increase were solely attributable to variations in the number of photoisomerizations. Significant fluctuations in the shape of the elementary response would cause the variance to have a shape different from that of the square of the mean. The scaling factor between the variance and the square of the mean indicated that the flash produced an average of 0.61 photoisomerizations.

fluctuations in the number of photoisomerizations is  $\bar{n}f^2(t)$ . Thus for an elementary response of fixed size and shape, the time-dependent variance is proportional to the square of the mean, and the constant of proportionality is the average number of photoisomerizations per flash. Fig. 4 C shows the variance for all of the responses contributing to the histogram in Fig. 4 A as well as the variance in darkness, which resulted from baseline drift, cellular dark noise, and instrumental noise. Assuming that the light-induced variance and the variance in darkness are independent and additive, the difference (light - dark) is the variance attributable to the flash response itself. This difference had the shape of the square of the mean response (Fig. 4 D). The scaling factor gave an average of 0.61 photoisomerizations per flash,

which is comparable to the estimate of 0.67 obtained by fitting the amplitude histogram of Fig. 4 A. In 11 of 16 cells the square of the mean response had the same shape as the variance increase. In the other five cells the variance during the response recovery was slightly greater than the square of the mean. In all cases fluctuations in the shape of the elementary response contributed much less to the variance than did Poisson fluctuations in the number of photoisomerizations.

What is the intrinsic time-dependent variance of the elementary response, separated from variance introduced by fluctuations in the number of photoisomerizations? This residual variability is generated by the phototransduction process and should further constrain the mechanism that

confers reproducibility. Elementary responses were isolated by the method used in constructing Fig. 4B. Fig. 5A shows the time-dependent variance of the elementary response and the variance in darkness from one such experiment. Precautions were taken to avoid systematic changes in the elementary response during the course of the experiment, as these would inflate the residual variance (see Materials and Methods). Fig. 5B shows the variance increase attributable to the elementary response and, for comparison, the square of the mean response (note different axis scales). The small resid-

ual variance of the elementary response is an upper limit to the intertrial variability of the signal triggered by a single photoisomerized rhodopsin. It appears to consist of two components, one reaching its maximum near the peak of the response and the other during the recovery phase. The relative magnitudes of these components differed from cell to cell. To pool measurements from multiple cells, the time and amplitude axes were normalized by the time to peak and square of the peak amplitude of the mean response; the normalized variance and mean response squared were then averaged (Fig. 5C, 12 cells). The variance was 15–20 times smaller than the square of the mean response until well after the peak of the response. The Discussion explores the implications of this small residual variability for possible mechanisms of reproducibility.

#### Time course of rhodopsin's catalytic activity

Experiments such as those in Figs. 3–5 quantify the reproducibility of the rod's elementary response. Before exploring possible mechanisms for reproducibility, we examined a general problem that bears upon all potential mechanisms: the time course of rhodopsin's catalytic activity. It has been suggested that rhodopsin deactivation dominates the rate of decline in PDE activity after a flash (Pepperberg et al., 1994; Corson et al., 1994) and, alternatively, that rhodopsin activity decays more quickly (Murnick and Lamb, 1996; Sagoo and Lagnado, 1997; Nikonov et al., 1998). The essential question for reproducibility is whether the amplitude alone or both the amplitude and the shape of the elementary response are sensitive to fluctuations in rhodopsin's catalytic activity. If the catalytic activity is confined to a brief time interval at the beginning of the response, variability in rhodopsin's activity should affect the response amplitude but not its shape. If, instead, the catalytic activity persists through a significant fraction of the elementary response, variability in the activity should affect both the response amplitude and shape. The experiments described below indicate that rhodopsin's activity persists through a significant fraction of the dim flash response in truncated outer segments at constant internal  $\text{Ca}^{2+}$ . We use this result in subsequent experiments to test the mechanisms responsible for reproducibility.

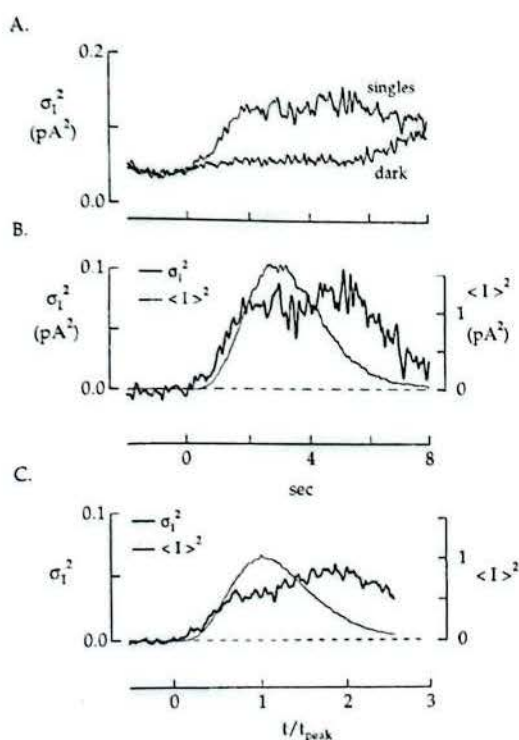


**FIGURE 5** Residual variability of the single photon response. (A) Time-dependent variance of 71 elementary responses ("singles") and 119 traces recorded in darkness ("dark"). Elementary responses were identified from a histogram of the response amplitudes as described in the text. Responses clearly contaminated by discrete noise events were excluded. The variance measured in darkness was caused by instrumental and cellular dark noise. The additional variance of the singles is due to intertrial variability in the elementary response. Current was collected from only the distal third of the outer segment to reduce the cellular dark noise. Light stimuli were applied over a 10  $\mu\text{m}$  wide slit centered on the region from which current was collected. The flash produced an average of 0.56 photoisomerizations. (B) Variance of the elementary response from A (thick trace) and square of the mean response (thin trace). Assuming that the variance of the singles and the dark variance were independent and additive, the variance in the elementary response could be isolated as the difference (singles – dark). Note that the peak of the variance is ~15 times smaller than the square of the mean. (C) Collected results from experiments on 12 cells. In each cell the variance and the square of the mean elementary response were measured as in A and B. Each measure was normalized by the time to peak and the square of the peak amplitude of the mean elementary response. The average of the normalized variance and square of the mean response are plotted. Note that the variance is ~15 times smaller than the square of the mean.

#### Time course of rhodopsin activity in truncated outer segments

The average time course of rhodopsin's catalytic activity was measured in truncated outer segments by abruptly increasing the gain of transducin activation by rhodopsin at specific times after a flash. The method for changing the gain is shown schematically in Fig. 6. Photoisomerized rhodopsin binds transducin-GDP and the GDP dissociates. The rhodopsin-transducin complex can then bind either GTP or GDP, but only GTP binding produces activated transducin. Thus transducin was activated with high gain when the solution dialyzing the outer segment contained 1

dialyzing  
dialysis

Combina  
la forma  
de la forma  
replicativa  
o de  
o  
la  
orden

de los segmentos  
funcionales?

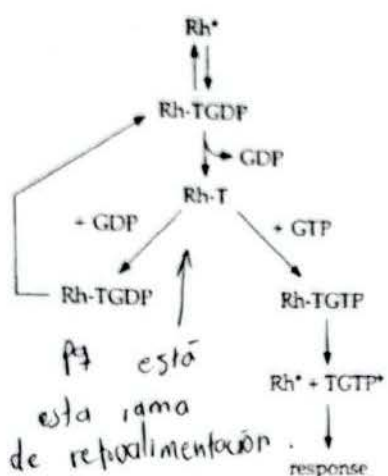


FIGURE 6 Procedure for changing rhodopsin-transducin gain. Photoisomerization promotes the binding of transducin-GDP to isomerized rhodopsin and the dissociation of GDP. This leaves the nucleotide binding site on transducin empty. Binding of GTP causes dissociation of rhodopsin-transducin and transducin activation. Binding of GDP simply returns rhodopsin-transducin to the initial state, from which rhodopsin and transducin-GDP or GDP alone can dissociate. Thus a high GDP concentration causes several futile cycles of GDP binding and unbinding for each transducin that is activated. **A high GTP concentration suppresses futile cycling and causes efficient transducin activation.** This procedure allows the gain of transducin activation to be lowered without using a very low GTP concentration, which alone could slow rhodopsin phosphorylation or arrestin binding and thus prolong the flash response (see Fig. 13). This procedure assumes that increasing the GTP concentration does not cause significant GDP-GTP exchange on the  $\alpha$  subunit of transducin; biochemical experiments (Fung, 1983) support this assumption.

mM GTP and 90  $\mu$ M GDP and with low gain when the dialyzing solution contained 10  $\mu$ M GTP and 90  $\mu$ M GDP. The addition of GDP to compete with GTP allowed the gain to be lowered without using an extremely low GTP concentration, which in the absence of GDP might slow rhodopsin shutoff (see Fig. 6 legend).

Fig. 7 shows results from one GTP-jump experiment. Initially the outer segment was dialyzed with the low-gain solution. A flash producing  $\sim$ 10 photoisomerizations was delivered, and the dialyzing solution was switched to the high-gain solution after a delay indicated in the upper trace. Responses with solution changes initiated 1, 2, and 8 s after the flash are superimposed in Fig. 7A (traces 1–3). Two control responses were also recorded: a flash response with the low-gain dialyzing solution (trace 4) and a response to the solution change alone to check for cGMP synthesis at the high GTP concentration (trace 5). As described below, rhodopsin's catalytic activity was estimated by linearizing each response and isolating the change in current produced by the increase in rhodopsin's ability to activate transducin.

We estimated rhodopsin's catalytic activity from records such as those in Fig. 7A by correcting for the nonlinear relations between the current and cGMP concentration and between the rate of change in cGMP concentration and rhodopsin activity. From Eqs. 2 and 8 the time derivative of the inward current,  $dI/dt$ , is related to the rates of cGMP

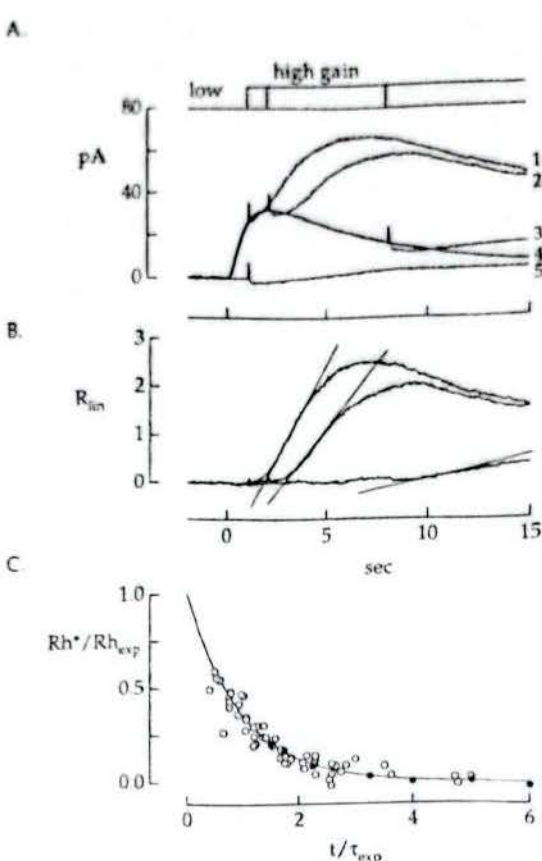


FIGURE 7 Time course of rhodopsin's catalytic activity measured by abruptly increasing the gain of transducin activation. (A) Original records from one such experiment. The outer segment was initially dialyzed with a solution containing 10  $\mu$ M GTP and 90  $\mu$ M GDP, giving low rhodopsin-transducin gain. At a specific time after a flash was delivered, the dialyzing solution was switched to one containing 1 mM GTP and 90  $\mu$ M GDP, giving high rhodopsin-transducin gain. In traces 1–3 this solution change was made 1, 2, and 8 s after the flash, as shown in the upper timing trace. Trace 4 is a flash response measured in the low-gain dialyzing solution. Trace 5 is the change in current produced by the solution change in the absence of a flash. Flash stimuli were applied over a 10  $\mu$ m wide transverse slit and produced  $\sim$ 60 photoisomerizations. The dark current was  $\sim$ 75 pA. (B) Linearized difference currents from A. Each of the responses in A was linearized (see text) to yield a proportional measure of rhodopsin activity. The two corrected control responses—the flash in the low gain solution (trace 4) and the current change produced by the solution change alone (trace 5)—were subtracted from the corrected responses to both the flash and solution change (traces 1–3). The initial slope of these corrected difference currents is proportional to rhodopsin's catalytic activity. (C) Collected results from 13 experiments. Results from each experiment have been normalized by the amplitude  $Rh_{exp}$  and time constant  $\tau_{exp}$  of the best fit exponential,  $Rh(t) = Rh_{exp} \exp(-t/\tau_{exp})$ . The mean time constant was  $2.3 \pm 0.2$  s (mean  $\pm$  SEM). Measurements from the experiment in A and B are plotted as filled circles.

synthesis and hydrolysis by

$$\frac{dI}{dt} = \frac{dI}{dG} \frac{dG}{dt} \quad (13)$$

$$= 3I[\gamma_{eff}/G - P_D - p_F] - 3p_S I,$$

where  $G$  is the cGMP concentration,  $\gamma_{eff}$  is the rate of cGMP diffusion into the outer segment from the dialyzing solution,

$P_D$  is the dark PDE activity,  $p_F$  is the light-evoked increase in PDE activity in the low-gain dialyzing solution, and  $p_S$  is the increment in PDE activity due to residual rhodopsin activity at the time of the solution change. The additional change in current 0.5–1 s after the solution change was relatively small and approximated a perturbation superimposed on the flash response. In this case the first term on the right side of Eq. 13 describes the current change produced by the flash response in the absence of the solution change, and the second term describes the additional change produced by increasing the rate of transducin activation. Thus the increment in PDE activity  $p_S$  produced by the solution change is proportional to  $(d \ln I/dt)_S$ , the contribution of the solution change to the slope of the logarithm of the current. As  $p_S$  varies linearly with the rhodopsin activity at a fixed time after the solution change (see Eq. 1), the rhodopsin activity is also proportional to  $(d \ln I/dt)_S$ . Each measured trace was corrected by computing the logarithm of the inward current at each instant of time; the two linearized control traces were then subtracted from the linearized trace with the solution change. The initial slope of the corrected difference current measures rhodopsin's catalytic activity (Fig. 7B). The slope was measured in a 0.25–0.5 s time window starting 0.25 s after the solution change. This analysis was repeated for several delays between the flash and solution change.

Rhodopsin activities  $Rh^*(t)$  measured in different outer segments were normalized by the amplitude  $Rh_{exp}$  and time constant  $\tau_{exp}$  of the best-fit exponential  $Rh_{exp} \exp(-t/\tau_{exp})$ , where  $t$  is the time between the flash and the slope measurement. Results from 13 experiments are collected in Fig. 7C. The average rhodopsin activity declined approximately exponentially over the range of times probed with a time constant of  $2.3 \pm 0.2$  s (mean  $\pm$  SEM). The time constant measured when the flash suppressed less than 30% of the dark current was similar to that when a brighter flash was used (2.1 s versus 2.5 s); thus the correction for the nonlinear relation between current and rhodopsin activity described above did not significantly influence  $\tau_{exp}$ . From these experiments we conclude that rhodopsin's catalytic activity in truncated outer segments declines on average with a time constant of 2–2.5 s. This relatively slow deactivation indicates that both the amplitude and shape of the elementary response should be sensitive to fluctuations in rhodopsin's activity.

Further evidence that rhodopsin's catalytic activity was relatively long-lived in truncated outer segments came from experiments in which phosphorylation was slowed by lowering the ATP concentration. If rhodopsin deactivated quickly, a slight prolongation of its activity would increase the amplitude of the dim flash response but would have relatively little effect on the time to peak. If rhodopsin's activity persisted through a significant fraction of the response, prolongation should have similar effects on the amplitude and time to peak. In seven outer segments in which dim flash responses were measured at 200 and 20  $\mu\text{M}$  ATP (e.g., Fig. 12), the time to peak increased by  $30 \pm 4\%$  in low ATP, whereas the peak amplitude increased by  $30 \pm 8\%$  (mean  $\pm$  SEM). Thus the time to peak and peak amplitude of the elementary response

were equally sensitive to slowing the time course of rhodopsin's catalytic activity, in agreement with the relatively slow deactivation profile measured in Fig. 7.

#### Comparison of deactivation kinetics in truncated and intact cells

A potential problem in the experiments described above is a slowing of rhodopsin shutoff due to diffusional loss of rhodopsin kinase or arrestin from the truncated outer segment. Three observations suggest that this was not significant during the 15–20 min period in which measurements were made. First, experiments described below indicate that neither phosphorylation nor arrestin binding dominated the time required for rhodopsin shutoff in truncated outer segments (Figs. 14 and 15). Second, the kinetics of dim flash responses measured in truncated outer segments with active cGMP synthesis were similar to those measured in intact cells at constant internal  $\text{Ca}^{2+}$  (see Materials and Methods): the time to peak and integration time were  $3.6 \pm 0.5$  s and  $7.9 \pm 1.7$  s in truncated outer segments and  $4.4 \pm 0.9$  s and  $7.1 \pm 1.3$  s in intact cells at constant internal  $\text{Ca}^{2+}$  (mean  $\pm$  SD, 11 truncated outer segments, 11 intact cells). Third, the 2.3 s time constant for the decline of rhodopsin's catalytic activity in truncated outer segments is similar to that of 2–2.5 s measured for the decline in PDE activity in intact cells after saturating flashes (Pepperberg et al., 1994; Corson et al., 1994; Lyubarsky et al., 1996; Murnick and Lamb, 1996) and estimated after a dim flash (below).

To estimate the rate of PDE shutoff in intact cells after a dim flash, we analyzed the kinetics of responses measured with the outer segment  $\text{Ca}^{2+}$  concentration held constant (see also Lyubarsky et al., 1996; Nikonov et al., 1998). From Eq. 2 the PDE activity during the flash response can be estimated from the cGMP concentration  $G(t)$ , the basal PDE activity  $P_D$ , and dark cGMP concentration  $G_D$  as

$$P(t) = \frac{P_D G_D - dG(t)/dt}{G(t)} \quad (14)$$

where at constant internal  $\text{Ca}^{2+}$  the synthesis rate has been written as  $\gamma = P_D G_D$ . Equation 14 neglects the effect of spatial inhomogeneities in the cGMP concentration, a valid approximation provided the change in current is related linearly to the change in cGMP.  $G(t)$  was estimated, using Eq. 9, from the average of 20–40 responses to a flash producing less than five photoisomerizations. The time course of the PDE activity was estimated from Eq. 14, assuming  $P_D = 0.1 \text{ s}^{-1}$  (Rieke and Baylor, 1996). Fig. 8 illustrates this analysis. Fig. 8A shows the average dim flash response of an intact cell with the internal  $\text{Ca}^{2+}$  held constant, and Fig. 8B shows the time course of the PDE activity calculated from this flash response. The light-activated PDE activity in this cell declined with a time constant of 2.1 s (*smooth curve* in Fig. 8B); in 11 cells the time constant was  $2.6 \pm 0.3$  s (mean  $\pm$  SEM). Thus after a dim flash, the PDE activity in an intact rod at constant  $\text{Ca}^{2+}$  declined at a rate similar to that of the decline

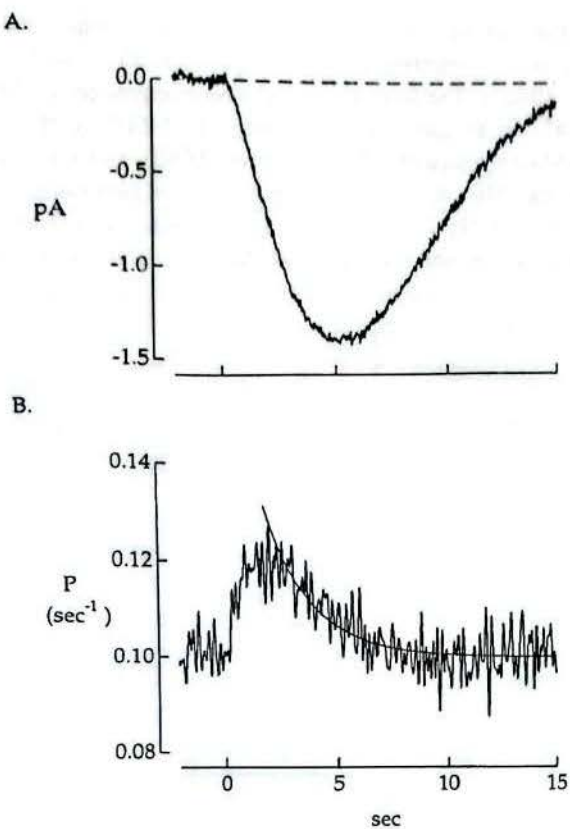


**FIGURE 8** Time course of PDE activity after a dim flash. (A) Average dim flash response in an intact cell measured at constant internal  $\text{Ca}^{2+}$  (see Materials and Methods). The flash produced an average of 1.2 photoisomerizations. The dark current was +9.5 pA. (B) Time course of PDE activity calculated according to Eq. 14 from the flash response in A, assuming a mean dark PDE activity of  $0.1 \text{ s}^{-1}$ . The smooth curve is an exponential with a time constant of 2.1 s fitted to the measured trace between 3 and 15 s.

in rhodopsin activity in a truncated outer segment. This suggests that rhodopsin's activity is relatively long-lived in both truncated outer segments and intact cells at constant internal  $\text{Ca}^{2+}$ .

#### Summary

The general conclusion from the experiments in this section is that rhodopsin's catalytic activity in truncated outer segments at constant  $\text{Ca}^{2+}$  persists through a significant fraction of the elementary response. Thus both the amplitude and shape of the response should be sensitive to fluctuations in rhodopsin's activity. Below we use the sensitivity of the response shape to fluctuations in rhodopsin's activity to test the mechanisms that might mediate reproducibility.

#### Possible mechanisms for reproducibility

Experiments such as those illustrated in Figs. 3–5 indicate that the entire waveform of the elementary response is reproducible. This is unexpected because the response originates from a single rhodopsin molecule whose active life-

time might be expected to fluctuate from trial to trial (see Introduction). Rhodopsin shutoff is thought to result from one or two phosphorylations followed by arrestin binding (Ohguro et al., 1995). If the time required for phosphorylation or arrestin binding were the dominant delay in rhodopsin deactivation, the distribution of catalytic lifetimes would be approximately exponential. If the amplitude of the photocurrent were proportional to rhodopsin's catalytic lifetime, the distribution of photocurrent amplitudes would also be nearly exponential. For the exponential distribution, the ratio of the mean  $\bar{A}$  to the standard deviation  $\sigma_A$  is 1, substantially less than the measured ratio of 5. The ratio  $\bar{A}/\sigma_A$  would increase only slightly (as the square root of the number of steps) if rhodopsin shutoff involved two or three steps with similar rate constants, and the increase in  $\bar{A}/\sigma_A$  would be less if the rate constants differed significantly. How, then, is such good reproducibility achieved? We tested the three possibilities outlined below.

#### Feedback control of single photon responses

An amplified product of photoisomerized, catalytically active rhodopsin could accumulate during the elementary response and act as a feedback signal that causes the response to terminate reproducibly. Such a feedback could reduce variability by regulating rhodopsin deactivation, or it could suppress the effects of variability in rhodopsin deactivation by acting at a later stage in the transduction cascade (Fig. 9 A). Several feedback pathways have been proposed to operate in phototransduction: acceleration of transducin shutoff by a reduction in the cGMP concentration (Arshavsky et al., 1992); acceleration of the rate of cGMP synthesis by the light-induced fall in  $\text{Ca}^{2+}$  (Koch and Stryer, 1988); and acceleration of rhodopsin shutoff by the fall in  $\text{Ca}^{2+}$  (Kawamura, 1993; Erickson et al., 1998) or by depletion of unactivated transducin near the active rhodopsin (Langlois et al., 1996).

#### Saturation

Saturation (Fig. 9 B) could reduce variability in the elementary response by making the photocurrent insensitive to intertrial fluctuations in rhodopsin's catalytic activity. For example, saturation might involve depletion of unactivated PDE on a single outer segment disk or closure of most or all of the cGMP-gated channels near the site of photon absorption.

#### Multiple steps in rhodopsin shutoff

Multiple steps in rhodopsin shutoff (Fig. 9 C) could cause the catalytic activity of each photoisomerized rhodopsin molecule to decline along a similar time course, leading to a reproducible elementary response. Fig. 9 C depicts each step as lowering rhodopsin's activity. This gradual decrease in the catalytic activity of a single molecule is consistent with the exponential decay of the average activity (Fig. 7).

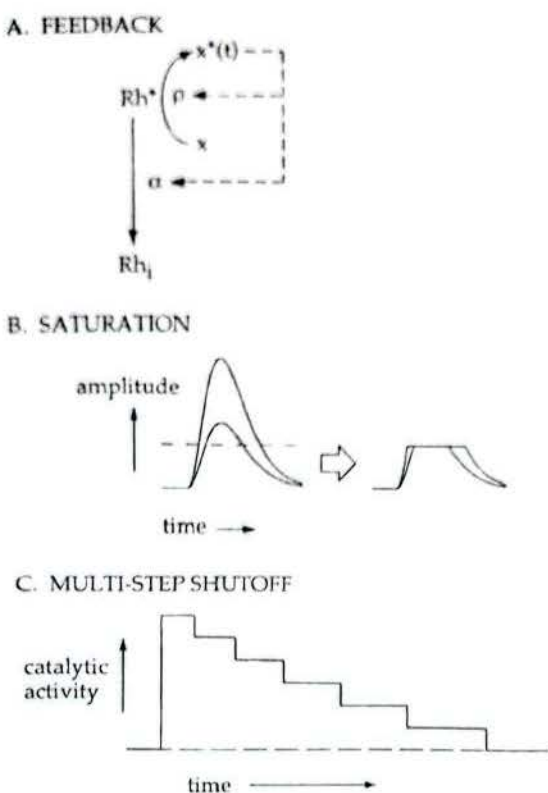


**FIGURE 9** Possible mechanisms for reproducibility. The low variability of the elementary response indicates either low intertrial variability in rhodopsin's catalytic activity or suppression of the effects of such variability by the transduction cascade. Three potential mechanisms are shown schematically. (*A*) A feedback signal  $x^*(t)$  might control the rate  $\alpha$  of rhodopsin shutoff or the rate  $\rho$  of activation of a downstream product of rhodopsin. Feedback control of rhodopsin shutoff could reduce intertrial variability in rhodopsin's activity, whereas feedback to a downstream element of the cascade could make the membrane current insensitive to variability in rhodopsin's activity. (*B*) A saturation might cause the membrane current to be insensitive to variability in rhodopsin's activity. A saturation acting at the peak of the response such as that depicted here (e.g., local depletion of open cGMP-gated channels) could reduce variability in the response amplitude. (*C*) Rhodopsin's catalytic activity might deactivate through a series of transitions, each of which reduces the activity by a small amount and occurs after a stochastic, first-order delay. Despite variations in the timing of individual transitions, variability in rhodopsin's cumulative activity could be reduced.

Shutoff through a series of  $n$  steps, each terminated by a first-order transition, would reduce variability in rhodopsin's activity by at most by  $1/\sqrt{n}$ . The measured reproducibility would thus require about 25 steps, far more than can be accounted for by the two known steps in rhodopsin shutoff—phosphorylation and arrestin binding (Lagnado and Baylor, 1992).

### Test of molecular mechanisms for reproducibility

#### Feedback

**$Ca^{2+}$  feedback.** A light-induced fall in the free  $Ca^{2+}$  concentration regulates several elements of the transduction cascade (reviewed by Koutalos and Yau, 1996). Suppress-

ing the fall in  $Ca^{2+}$  slows the dim flash response and increases its amplitude (Matthews et al., 1988; Nakatani and Yau, 1988a). The best documented consequence of the fall in  $Ca^{2+}$  is an increase in the rate of cGMP synthesis by guanylate cyclase (Koch and Stryer, 1988), but  $Ca^{2+}$  feedback can also act on the time course (Kawamura, 1993; Erickson et al., 1998; Sagoo and Lagnado, 1997) and the gain (Lagnado and Baylor, 1994; Murnick and Lamb, 1996) of rhodopsin's catalytic activity. Does  $Ca^{2+}$  feedback make the elementary response reproducible?

We tested for such a role of  $Ca^{2+}$  feedback by comparing dim flash responses from intact cells with the internal  $Ca^{2+}$  concentration held constant or freely changing (see Materials and Methods). The single photon response slowed and increased in amplitude when light-induced changes in internal  $Ca^{2+}$  were suppressed (Fig. 10 *A*). Nevertheless, responses to zero, one, and two photoisomerizations had distinguishable amplitudes (Fig. 10 *B*). In four cells enough responses were collected at constant internal  $Ca^{2+}$  to construct amplitude histograms; in these cells the ratio of the elementary response amplitude  $\bar{A}$  to its standard deviation  $\sigma_A$  was  $5 \pm 2$  (mean  $\pm$  SD), not significantly different from the ratio when the  $Ca^{2+}$  changed freely. Further evidence for low variability of the elementary response at constant  $Ca^{2+}$  came from comparing the time-dependent variance increase to the square of the mean response. In all nine cells tested, Poisson fluctuations in the number of photons absorbed dominated the variance. In four of nine cells, the shape of the variance increase was similar to the square of the mean response. In the other five cells there was additional variance during the later part of the response (e.g., Fig. 10 *C*); this additional variance in the elementary response could have arisen from genuine variability in the elementary response or from intertrial variability in the procedure used to suppress changes in  $Ca^{2+}$ . In all nine experiments the scaling factor between the variance increase and the square of the mean response differed by <20% between runs with the internal  $Ca^{2+}$  held constant and with the  $Ca^{2+}$  changing freely. These results indicate that reproducibility was substantially maintained without  $Ca^{2+}$  feedback.

Analysis of responses at constant  $Ca^{2+}$  in truncated outer segments pointed to the same conclusion. Here it was not possible to collect enough responses for an amplitude histogram, and instead the time-dependent variance increase and the square of the mean response were compared. As in intact cells, the variance increase and square of the mean had similar shapes (e.g., see Fig. 17 *A*), indicating that the time course of the elementary response was reproducible.

Experiments such as those in Figs. 10 and 17 indicate that  $Ca^{2+}$  feedback speeds the recovery of the response but is not required for reproducibility.

**Feedback pathways not based on  $Ca^{2+}$ .** We tested for a larger class of feedback signals that might control rhodopsin shutoff, using the strategy shown schematically in Fig. 11 *A*. If the deactivation of rhodopsin's catalytic activity is regulated by a feedback signal  $x(t)$  originating at or downstream

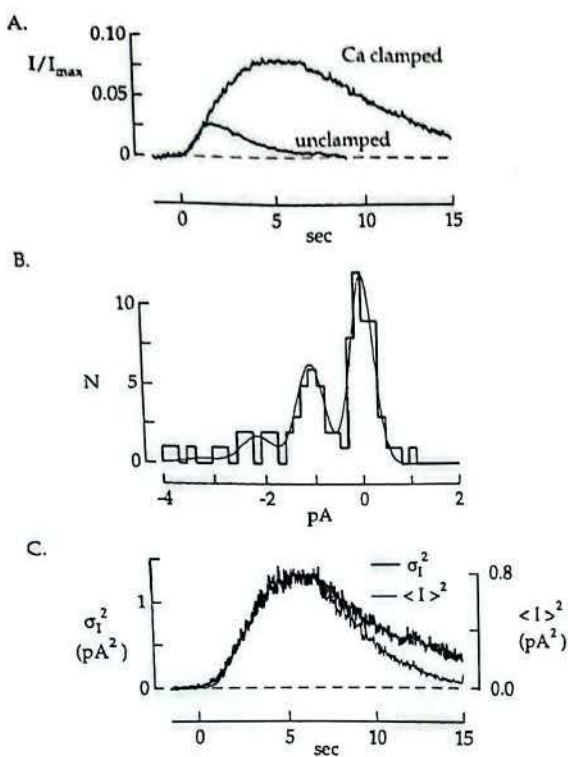


**FIGURE 10** Single photon responses at constant internal  $\text{Ca}^{2+}$ . (A) Comparison of average dim flash responses measured with the  $\text{Ca}^{2+}$  allowed to change normally and with the  $\text{Ca}^{2+}$  held constant near its normal concentration in darkness (see Materials and Methods). Responses have been normalized by the dark current, which was  $-26 \text{ pA}$  with the  $\text{Ca}^{2+}$  changing freely and  $+10 \text{ pA}$  with the  $\text{Ca}^{2+}$  held constant. The flash produced an average of  $0.6$  photoisomerizations. (B) Amplitude histogram from  $83$  dim flash responses measured at constant internal  $\text{Ca}^{2+}$ . The amplitudes are negative because responses were inverted when the outer segment was superfused with the  $0 \text{ Na}^+$ , low  $\text{Ca}^{2+}$  solution (see Materials and Methods). Peaks corresponding to  $0$  and  $1$  photoisomerization can be clearly distinguished. The smooth curve was calculated according to Eq. 11 with  $A = -1.1 \text{ pA}$ ,  $\sigma_A = 0.25 \text{ pA}$ ,  $\sigma_D = 0.14 \text{ pA}$ , and  $\bar{n} = 0.61$  photoisomerizations per flash. The mean response is shown in A. (C) Time-dependent variance increase (thick trace) and square of the mean response (thin trace) for responses contributing to the amplitude histogram in B. The light-dependent variance increase has been isolated by subtracting the variance measured in darkness from that measured from the flash responses, as in Fig. 4 C. The scaling factor between the variance and the square of the mean indicated an average of  $0.59$  photoisomerizations per flash.

from active transducin, then the rate at which the feedback signal accumulates will be altered when the rhodopsin-transducin gain is changed. Slowing the accumulation of the feedback signal should delay the feedback effect and prolong rhodopsin's catalytic activity. Because rhodopsin deactivates relatively slowly (Fig. 7), prolonging rhodopsin's activity should prolong the dim flash response. The internal  $\text{Ca}^{2+}$  was held constant in these experiments (see Materials and Methods) to eliminate  $\text{Ca}^{2+}$  feedback.

The rhodopsin-transducin gain was altered by changing the GTP/GDP ratio (see Fig. 6). The high-gain dialyzing solution contained  $90 \mu\text{M}$  GTP and  $10 \mu\text{M}$  GDP, and the low-gain solution contained  $90 \mu\text{M}$  GDP and  $10 \mu\text{M}$  GTP.

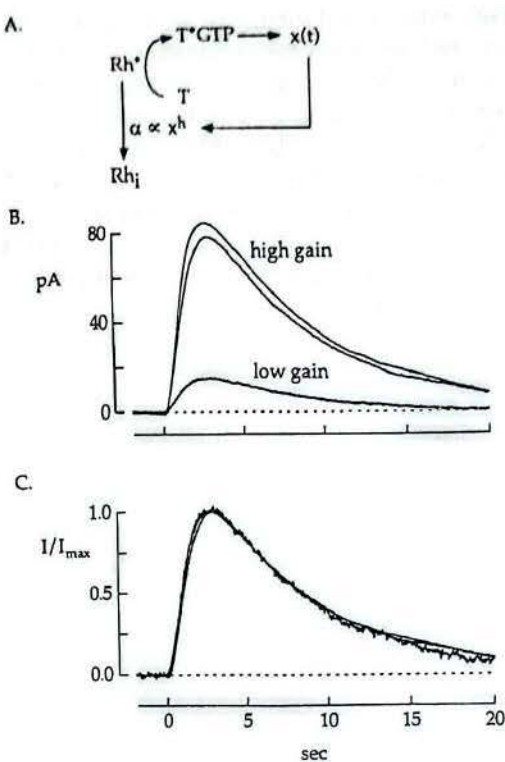


**FIGURE 11** Test for feedback control of rhodopsin shutoff. (A) Experimental rationale. If rhodopsin shutoff is controlled by feedback from an activation product  $x$  of transducin, then lowering the rate of transducin activation should slow the accumulation of  $x$  and thus slow rhodopsin shutoff. As the shape of the dim flash response is sensitive to the time course of rhodopsin's activity, the presence of such a feedback should cause the shapes of dim flash responses at high and low rates of transducin activation to differ. (B) Dim flash responses measured in a truncated outer segment dialyzed with  $90 \mu\text{M}$  GDP and  $10 \mu\text{M}$  GTP, producing low rhodopsin-transducin gain (thick trace), or  $90 \mu\text{M}$  GTP and  $10 \mu\text{M}$  GDP, producing high gain (thin traces). The dialyzing solution contained  $500 \mu\text{M}$  ATP in both cases. The response at low gain was measured between the two at high gain. This manipulation changed the rate of transducin activation by a factor of  $5$ , as judged by the slope of the rising phase of the flash response. The dark current was  $-160 \text{ pA}$ . Flash stimuli producing  $\sim 15$  photoisomerizations were applied over a  $10 \mu\text{m}$  wide transverse slit. (C) Responses at low and high gain from B scaled by their respective peak amplitudes. Despite the different rates of transducin activation, the response kinetics were not measurably different. This relative insensitivity of the response kinetics to changes in the rate of transducin activation indicates that rhodopsin's catalytic lifetime is not regulated by a feedback originating at or downstream of active transducin.

Changing the gain reversibly altered the amplitude of the dim flash response (Fig. 11 B) but did not change the response shape, as demonstrated by scaling each response by its peak amplitude (Fig. 11 C). A similar invariance of the response kinetics to a change in the rhodopsin-transducin gain was observed in each of five experiments. The gain, as judged by the initial rate of rise of the flash response, changed on average by a factor of  $4.5$  (range  $3.1$ – $6.1$ ), whereas the time to peak changed by less than  $5\%$  in each experiment. These results indicate that rhodopsin deactivation is not under feedback control by transducin or any of its activation products, and therefore that such a feedback does

not explain the reproducibility of the elementary response.  $\text{Ca}^{2+}$  is excluded from this argument, as its internal concentration was held constant in these experiments.

**Summary.** The conclusion from this section is that reproducibility is not mediated by  $\text{Ca}^{2+}$  feedback to any element of the cascade (Figs. 10 and 17), nor is it mediated by any other feedback signal that controls rhodopsin shutoff and originates at or after active transducin (Fig. 11). In the Discussion we return to other potential feedback pathways that might contribute to reproducibility.

#### Saturation

A saturation—e.g., activation of all the PDE on a single outer segment disk or closure of all of the channels in a local region of the outer segment membrane—might make the elementary response reproducible by rendering the membrane current insensitive to variations in the time course of rhodopsin's catalytic activity. Such a saturation would manifest itself as a time-dependent nonlinearity, causing the current to become relatively independent of rhodopsin's activity. Several manipulations are known to increase the elementary response amplitude, including holding the internal  $\text{Ca}^{2+}$  constant (Matthews et al., 1988; Nakatani and Yau, 1988a; Fig. 10 A) and slowing or disabling rhodopsin phosphorylation (Palczewski et al., 1992; Chen et al., 1995); these observations indicate that complete saturation does not occur. The experiments presented below provide evidence against partial saturation as an explanation for reproducibility.

We compared the change in the dim flash response in truncated outer segments upon prolonging rhodopsin's activity with the change expected if the cascade responded linearly to rhodopsin activity—i.e., without saturation. Rhodopsin shutoff was slowed by lowering the ATP concentration in the dialyzing solution from 200  $\mu\text{M}$  to 20  $\mu\text{M}$  to slow rhodopsin phosphorylation. This manipulation increased the amplitude and slowed the kinetics of the dim flash response (Fig. 12 A). To determine whether lowering the ATP concentration indeed slowed rhodopsin shutoff, rhodopsin's catalytic activity was measured by the procedure in Fig. 7 5 s after a flash was delivered at high and low ATP; the activity in 20  $\mu\text{M}$  ATP was about twice that in 200  $\mu\text{M}$  ATP (two cells, data not shown). Fig. 12 B shows the expected effect of prolonging rhodopsin shutoff on the dim flash response, calculated using the linear model described in Eqs. 6 and 10. Rhodopsin's catalytic activity was assumed to decline exponentially with a time constant of 2.5 s at high ATP and 5 s at low ATP. The measured and calculated dim flash responses exhibited similar changes in amplitude and time to peak, indicating that significant saturation did not occur.

Further evidence that saturation cannot explain reproducibility is provided by the low variability of the response shape in both intact cells and truncated outer segments (see Figs. 4 D, 5 C, and 17 A). The relatively long duration of rhodopsin's catalytic activity in truncated cells at constant

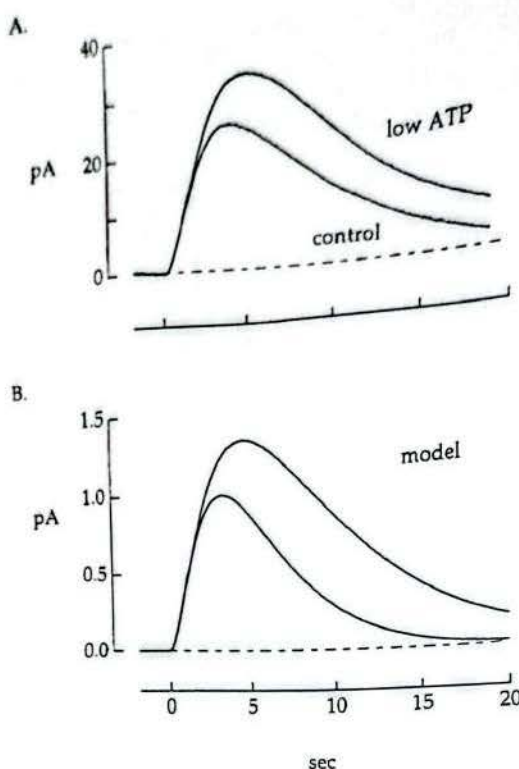


FIGURE 12 Test for saturation of the elementary response in a truncated outer segment. (A) Lowering the ATP concentration slowed and increased the amplitude of the dim flash response. The traces show average dim flash responses measured in a truncated outer segment dialyzed with a solution containing 1 mM GTP, 300 nM free  $\text{Ca}^{2+}$ , and either 200  $\mu\text{M}$  ATP (control) or 20  $\mu\text{M}$  ATP (low ATP). The dark current was  $-140 \text{ pA}$ , and the flash produced an average of six to seven photoisomerizations. (B) Predicted change in flash response from the linear model described in Eqs. 6 and 10, assuming a basal PDE activity of  $0.1 \text{ s}^{-1}$  and an exponential decay of rhodopsin's catalytic activity, with a time constant of 2.5 s at high ATP and 5 s at low ATP.

internal  $\text{Ca}^{2+}$  (Fig. 7) indicates that the shape of the response should be sensitive to fluctuations in the time course of rhodopsin shutoff. A simple amplitude saturation should reduce variability only at the peak of the response; other types of saturation would similarly be expected to affect only part of the response.

Although these experiments do not rule out the possibility that saturation contributes to reproducibility, they show that saturation alone cannot account for it.

#### Multistep rhodopsin shutoff

Deactivation through a series of states, each terminated by a stochastic transition, could reduce intertrial variability in rhodopsin's catalytic activity (Fig. 9 C). To minimize variability, the product of the average activity and mean duration should be equal for each state, so that each controls the same fraction of rhodopsin's cumulative activity. If one state dominated, rhodopsin shutoff would effectively be controlled by a single transition and would exhibit large

intertrial variability. This model makes two testable predictions: 1) the known transitions in rhodopsin shutoff—phosphorylation and arrestin binding—cannot control a large fraction of rhodopsin's cumulative activity; and 2) variability in the elementary response should increase if a single transition is slowed so that the preceding state accounts for much of rhodopsin's cumulative activity.

**Contributions of phosphorylation and arrestin binding.** The known transitions in the shutoff of rhodopsin's catalytic activity are the binding of rhodopsin kinase, incorporation of a phosphate in rhodopsin's C terminus by the kinase, and the binding of arrestin. We will refer to kinase binding and the subsequent incorporation of a phosphate as phosphorylation. Several studies indicate that phosphorylation initiates response recovery (Nakatani and Yau, 1988c; Chen et al., 1995). Indeed, dim flash responses in truncated outer segments dialyzed with a solution lacking ATP rose to a plateau that was maintained for at least 30 s (four experiments; data not shown). Similarly, arrestin binding provides complete deactivation of rhodopsin's catalytic activity (Bennett and Sitaramayya, 1988; Xu et al., 1997). Experiments described below indicate that these requisite first and last steps in rhodopsin deactivation control only a small part of the integrated activity.

Kinase, arrestin, and transducin bind competitively to rhodopsin (Miller and Dratz, 1984; Krupnick et al., 1997). Thus while rhodopsin is bound to transducin it cannot be phosphorylated, nor can arrestin bind. The dissociation rate of rhodopsin-transducin, and hence the fraction of time rhodopsin is available for phosphorylation and arrestin binding, depend on the GTP concentration (Fig. 13); if the GTP concentration is sufficiently low, rhodopsin spends most of its time bound to transducin. This slowing in the dissociation rate of rhodopsin-transducin lowers the rate of transducin activation and thus the slope of the rising phase of the flash response, while at the same time decreasing the accessibility of rhodopsin for kinase and arrestin binding. If phosphorylation or arrestin binding controls most of rhodopsin's cumulative activity, lowering the GTP would slow rhodopsin shutoff and increase the time to peak of the response.

Fig. 14 A shows dim flash responses measured in a truncated outer segment dialyzed with 500  $\mu$ M ATP and 10 or 4  $\mu$ M GTP, concentrations low enough to prevent significant cGMP synthesis (Lagnado and Baylor, 1994; Rieke and Baylor, 1996). Lowering the GTP concentration from 10 to 4  $\mu$ M decreased the response amplitude but did not change the time to peak, as shown in Fig. 14 B, where the responses are scaled by their peak amplitudes. Thus the rate of transducin activation, and hence the rates of phosphorylation and arrestin binding, can be decreased significantly, apparently without changing the rate of rhodopsin shutoff. In the same outer segment, use of a dialyzing solution containing 20  $\mu$ M ATP provided a check that lengthening the lifetime of the rhodopsin-transducin complex slowed phosphorylation. Lowering the ATP concentration from 500 to 20  $\mu$ M slowed the flash response, indicating that at low ATP phosphorylation controlled a significant fraction of rhodopsin's cumulative

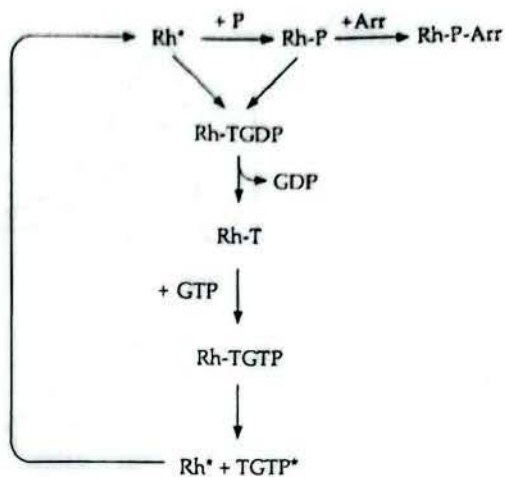


**FIGURE 13** Procedure for testing the contributions of kinase and arrestin binding to the time course of rhodopsin shutoff. Rhodopsin kinase and arrestin compete with transducin for a single binding site on rhodopsin. Thus while rhodopsin is bound to transducin, it is not accessible to the kinase or arrestin. In the absence of GDP, the dissociation rate of rhodopsin-transducin is determined by the GTP concentration; lowering the GTP concentration slows dissociation of rhodopsin-transducin and thus slows the binding of kinase and arrestin. The rate of transducin activation, measured from the initial slope of the flash response, indicates how much kinase and arrestin binding have been slowed. This maneuver should slow the deactivation of rhodopsin's catalytic activity and the shape of the dim flash response if either the kinase or the arrestin binding rate limits rhodopsin shutoff.

activity (see also Fig. 12). Under these conditions, lowering the GTP concentration changed both the rising phase and time to peak of the flash response (Fig. 14, C and D). In five similar experiments, reducing the GTP concentration from 10 to 4–5  $\mu$ M affected both the response amplitude and time to peak at low ATP, but only the amplitude at high ATP.

To collect results from multiple experiments such as that in Fig. 14, each response was fitted using the model described by Eqs. 6 and 10. The fitted parameters were the initial rate of transducin activation  $\sigma$  and the rate of rhodopsin deactivation  $\alpha$ , which were chosen to minimize the mean square error between the measured and calculated response; the other parameters of the model were held fixed at the values given in Theory.  $\sigma$  and  $\alpha$  were normalized in each experiment by the values for the fit to the response measured at 10  $\mu$ M GTP. Results from 18 outer segments dialyzed with 500  $\mu$ M ATP are collected in Fig. 15, which plots the normalized rate of rhodopsin shutoff against the normalized rate of transducin activation. If phosphorylation or arrestin binding limited the time course of rhodopsin deactivation, lowering the rate of transducin activation by a factor of  $a$  would slow rhodopsin deactivation by the same factor, and the points would fall along the line of slope 1. The points fall above this line, indicating that the rate of rhodopsin deactivation was relatively insensitive to slowing phosphorylation and arrestin binding. Thus the experiments summarized in Fig. 15 indicate that the time required for phosphorylation and arrestin binding cannot account for the time course of rhodopsin's catalytic activity.

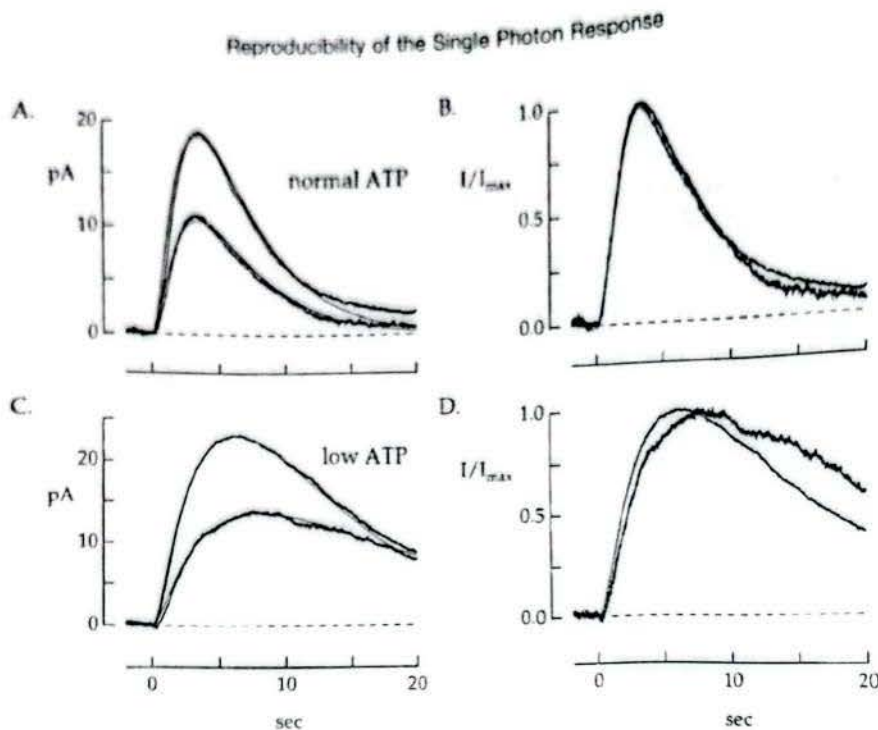


**FIGURE 14** Time required for phosphorylation and arrestin binding failed to explain the time course of rhodopsin's catalytic activity. The dark current was 80 pA. Flash stimuli producing ~10 photoisomerizations were applied over a 10  $\mu\text{m}$  wide transverse slit. (A) Averaged dim flash responses (10–15 trials) measured in a truncated outer segment dialyzed with 500  $\mu\text{M}$  ATP and 10 or 4  $\mu\text{M}$  GTP. Lowering the GTP concentration decreased the slope of the rising phase of the flash response, as expected for a decreased rate of transducin activation. The time to peak of the response, however, changed relatively little. The smooth traces were calculated according to Eqs. 6 and 10, assuming that rhodopsin's catalytic activity declined with an exponential time course. The fits were obtained by varying the rate constants for rhodopsin shutoff and transducin activation. Fits to the responses at high and low GTP were calculated using identical time constants for rhodopsin shutoff (2.1 s), whereas the rate of transducin activation was decreased by a factor of 1.8 at low GTP. (B) Responses from A scaled by their peak amplitudes to facilitate comparison of the response kinetics. (C) Control responses measured in the same outer segment. These responses, measured before those in A, were measured while the outer segment was dialyzed with 20  $\mu\text{M}$  ATP and, again, either 10 or 4  $\mu\text{M}$  GTP. Lowering the ATP slowed the flash response, presumably by slowing the rate of binding of kinase-ATP to active rhodopsin. In this case lowering the GTP concentration affected both the slope of the rising phase and the time to peak of the response. This result is expected if kinase binding is rate limiting at low ATP and stabilizing rhodopsin-transducin does indeed further slow kinase binding. Smooth traces fit to the measured responses were calculated as described in A, using a rhodopsin shutoff rate of 8.3 s at high GTP and 16.6 s at low GTP and a decrease in the rate of transducin activation by a factor of 2.1 at low GTP. (D) Scaled responses from C.

Phosphorylation accounts for a small fraction of rhodopsin deactivation. A second experiment tested the role of phosphorylation in rhodopsin shutoff. The timing of phosphorylation was controlled by removing ATP from a truncated outer segment to disable phosphorylation, delivering a flash, and then supplying ATP only during a brief time window near the peak of the response. Experiments were carried out at 5–8°C to slow the response relative to diffusion and allow effective removal of ATP during the flash response. Responses recovered fully when the outer segment was dialyzed with ATP for 10 s beginning at the time of the flash (Fig. 16 A, thick trace), recovery being identical to that when ATP was present throughout (Fig. 16 A, thin trace). Removal of ATP 10 s before a dim flash eliminated the response recovery (Fig. 16 B). As the response reached a peak in less than 10 s, ATP removal disabled phosphorylation in less than 20 s. Thus phosphorylation was restricted to a time window of at most 30 s after the flash in the experiment of Fig. 16 A, and much of the response recovery took place after phosphorylation had occurred. Similar results were observed in six outer segments.

The significance of these results for rhodopsin shutoff depends critically on whether rhodopsin's activity persists

throughout the flash response at low temperatures or whether another process is responsible for the slow recovery. In particular, lowering the temperature could slow transducin's GTPase activity, causing it to limit the rate of PDE deactivation after a flash. A lower bound to the rate of PDE deactivation was obtained by delivering a flash in the absence of ATP, waiting for the response to reach a plateau, and then disabling transducin activation by removing GTP from the dialyzing solution. Upon removal of GTP, the dark current recovered with a time constant determined by the decay of activated PDE and the time required for GTP to diffuse from the outer segment. At 5–8°C recovery upon GTP removal was faster than the normal recovery of the flash response in the presence of ATP (exponential time constant of  $27 \pm 4$  s versus  $57 \pm 9$  s, mean  $\pm$  SEM in six outer segments). Thus neither the time required for transducin and PDE shutoff nor that required for diffusion limited the response recovery, suggesting that rhodopsin continued to activate transducin throughout much of the response.

These results indicate that at low temperatures phosphorylation is a requisite step in the initiation of rhodopsin

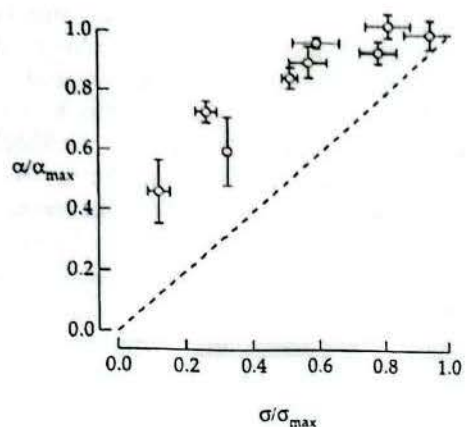


FIGURE 15 Collected results on the contributions of phosphorylation and arrestin binding to the time course of rhodopsin shutoff. The normalized rate of rhodopsin shutoff  $\alpha$  is plotted against the rate of transducin activation  $\sigma$  from 18 experiments. Responses at GTP concentrations ranging from 0.5 to 10  $\mu\text{M}$  were measured and fitted as in Fig. 14 to obtain estimates of the rate constants for rhodopsin shutoff and transducin activation. These rate constants were normalized by the estimates  $\alpha_{\max}$  and  $\sigma_{\max}$  from responses at 10  $\mu\text{M}$  GTP to compare responses across cells; each point represents the mean  $\pm$  SD from at least three measurements. All of the points fall above the dashed line, which represents the expectation if the rate of rhodopsin shutoff and rate of transducin activation were equally sensitive to a change in the GTP concentration. The relative insensitivity of the rate of rhodopsin shutoff to changes in the GTP concentration indicates that the time course of rhodopsin shutoff is not limited by phosphorylation or arrestin binding.

shutoff, but itself controls only a small fraction of rhodopsin's integrated activity.

*Increased variability when phosphorylation is rate limiting.* A second prediction of the multistep model for rhodopsin deactivation is that variability in the elementary response should increase if one step in rhodopsin shutoff is made rate limiting. This prediction was tested by slowing rhodopsin phosphorylation and examining the time-dependent variance of the dim flash response. Interleaved groups of 5–10 dim flash responses at 200 and 20  $\mu\text{M}$  ATP were recorded in a truncated outer segment, with a minimum of 20 responses recorded in each condition. Averaged responses at 200 and 20  $\mu\text{M}$  ATP are shown in Fig. 12. At high ATP the light-dependent variance increase was well described by the square of the mean response (Fig. 17 A), consistent with a reproducible elementary response and Poisson fluctuations in the number of absorbed photons. At low ATP the variance increase was considerably larger (Fig. 17 B). A similar increase in variance at low ATP was observed in five experiments. In each experiment the increase in variance was comparable to the variance introduced by the Poisson statistics of photon absorption, and thus accurate photon counting was not possible at low ATP. The increased variance at low ATP can be explained if rhodopsin's activity became more variable when phosphorylation limited rhodopsin deactivation.

The increased variance at low ATP can be compared to that expected from a simple stochastic model of rhodopsin

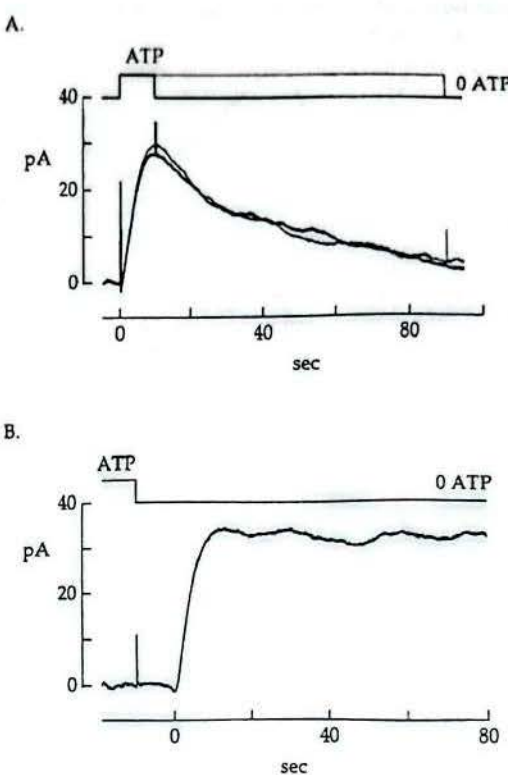
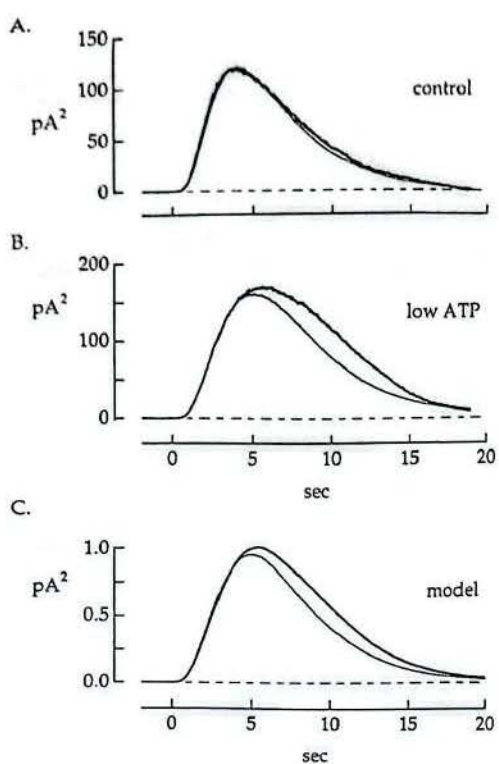


FIGURE 16 Contribution of phosphorylation to the shutoff of rhodopsin's catalytic activity. Dim flash responses were recorded from a truncated outer segment at 8°C dialyzed with a solution containing either 0 or 40  $\mu\text{M}$  ATP. The timing of the changes in the dialyzing solution is given in the upper traces. The dark current was  $-75$  pA. Flash stimuli producing  $\sim 80$  photoisomerizations were applied over a 10  $\mu\text{m}$  wide transverse slit. (A) Superimposed responses when the outer segment was dialyzed with ATP for 10 s or 90 s after the flash. The presence of ATP for a relatively brief time near the peak of the response was sufficient for a normal recovery. Thus phosphorylation was required for the initiation of recovery but did not itself much decrease rhodopsin's catalytic activity. (B) Response to a flash delivered 10 s after removal of ATP from the dialyzing solution. No recovery was evident, indicating that removal of ATP effectively suppressed phosphorylation and rhodopsin shutoff. As the response reached a peak in  $\sim 10$  s, this indicates that effective ATP removal required 20 s at most.

shutoff and the linear model for the transduction cascade described in Eqs. 6 and 10. Phosphorylation was assumed to act as a single-step process described by a time constant  $\tau_p$ , and the remainder of rhodopsin shutoff was assumed to be deterministic. At low ATP,  $\tau_p$  was assumed to account for half of the time course of rhodopsin shutoff. The average number of photoisomerizations was fixed by the measured scaling factor between the variance increase and square of the mean response. Fig. 12 shows the average flash responses calculated for these conditions. Fig. 17 C shows the calculated square of the mean response and time-dependent variance for a flash producing an average of seven photoisomerizations. The calculated increase in variance is similar to the measurements in Fig. 17 B. Thus variability of the elementary response increased by an amount consistent with the increase in rhodopsin's variability when its shutoff proceeded effectively as a one- or two-step process.

## Reproducibility of the Single Photon Response



**FIGURE 17** The elementary response variance increased when rhodopsin shutoff slowed. The dark current was  $-140$  pA. Flash stimuli were applied over a  $10\text{ }\mu\text{m}$  wide transverse slit. (A) Time-dependent variance increase (thick trace) and square of mean response (thin trace) from 22 trials when the outer segment was dialyzed with  $200\text{ }\mu\text{M}$  ATP and  $1\text{ mM}$  GTP. The scaling factor between the variance and the square of the mean indicated an average of six photoisomerizations per trial. (B) Variance increase and square of mean from 29 trials when the outer segment was dialyzed with  $20\text{ }\mu\text{M}$  ATP and  $1\text{ mM}$  GTP. The scaling factor between the variance and the square of the mean indicated an average of seven photoisomerizations per trial. (C) Variance and square of the mean response calculated according to Eqs. 6 and 10, assuming that on average the time required for phosphorylation accounted for half of rhodopsin's cumulative activity. Phosphorylation was modeled as a memoryless, first-order transition with a time constant  $\tau_p$  of  $2.5$  s. Rhodopsin deactivation after phosphorylation was assumed to follow a deterministic, exponential time course with a time constant of  $2.5$  s. The variance was calculated from 500 responses.

**Summary.** The relatively long time course of rhodopsin's catalytic activity (Fig. 7) and the inability of phosphorylation and arrestin binding to account for this time course (Figs. 14–16) indicate that additional steps contribute to rhodopsin deactivation. The increased variance in the elementary response when phosphorylation was rate limiting for rhodopsin shutoff (Fig. 17) indicates that the measured current was sensitive to variability in rhodopsin's activity. These results suggest that a reproducible deactivation process involving multiple transitions may occur between phosphorylation and arrestin binding.

## DISCUSSION

### Summary

We tested three possible mechanisms for the reproducibility of the rod's elementary response: 1) feedback to rhodopsin

or a downstream element of the cascade; 2) saturation of an activation product of rhodopsin; and 3) multistep deactivation of rhodopsin. The results indicate that reproducibility is not explained by saturation, by  $\text{Ca}^{2+}$  feedback of any kind, or by control of rhodopsin shutoff by a feedback signal originating at or after active transducin. We did not directly test three possible mechanisms: 1) feedback from a signal other than  $\text{Ca}^{2+}$  to an activation product of rhodopsin; 2) feedback control of rhodopsin shutoff by a molecular species activated in parallel with transducin; and 3) decay of rhodopsin's catalytic activity through a series of steps. We now discuss each of these possibilities.

### Feedback to cascade downstream of rhodopsin

A feedback acting downstream of rhodopsin from a signal other than  $\text{Ca}^{2+}$  could conceivably make the membrane current insensitive to variability in rhodopsin's catalytic activity. This seems unlikely, however, for several reasons. First, the low variability of the elementary response would require the feedback to be quite powerful. In the absence of phosphorylation the elementary response rises to a maintained plateau (Chen et al., 1995; Fig. 16), whereas a powerful feedback controlling amplification should cause at least some response recovery. Second, the increase in the mean and variance of the current when rhodopsin shutoff was slowed is consistent with calculations that assume that the membrane current is fully sensitive to variability in rhodopsin's activity (Fig. 17). Thus although feedback signals other than  $\text{Ca}^{2+}$  may control amplification, they probably do not mediate the reproducibility of the elementary response.

### Feedback to rhodopsin originating before active transducin

Regulation of rhodopsin shutoff by feedback from a molecular species activated in parallel with transducin might conceivably explain reproducibility. Such a mechanism must meet two requirements to be effective: 1) the molecule mediating the feedback must accumulate rapidly, so that variability in the feedback signal itself is small; and 2) the rate of rhodopsin shutoff must be highly sensitive to the amplitude of the feedback signal. Even if the feedback signal were effectively deterministic, it would have to exert its effect on a single photoisomerized rhodopsin molecule, presumably by binding to it. Stochastic fluctuations in the binding reaction set a limit to the effectiveness of this mechanism, as shown in Fig. 18, which compares the calculated time-dependent variance of the elementary response with the measured variance from Fig. 5. The feedback signal was assumed to have negligible variability, to accumulate linearly with time after photoisomerization, and to act with a cooperativity  $h$  on the rate  $\alpha$  of rhodopsin shutoff—i.e.,  $\alpha \propto t^h$ . The time-dependent variance of the elementary response was calculated using the model described in Eqs. 7 and 10. Higher cooperativities caused the rhodopsin shutoff rate to increase more abruptly and thus were

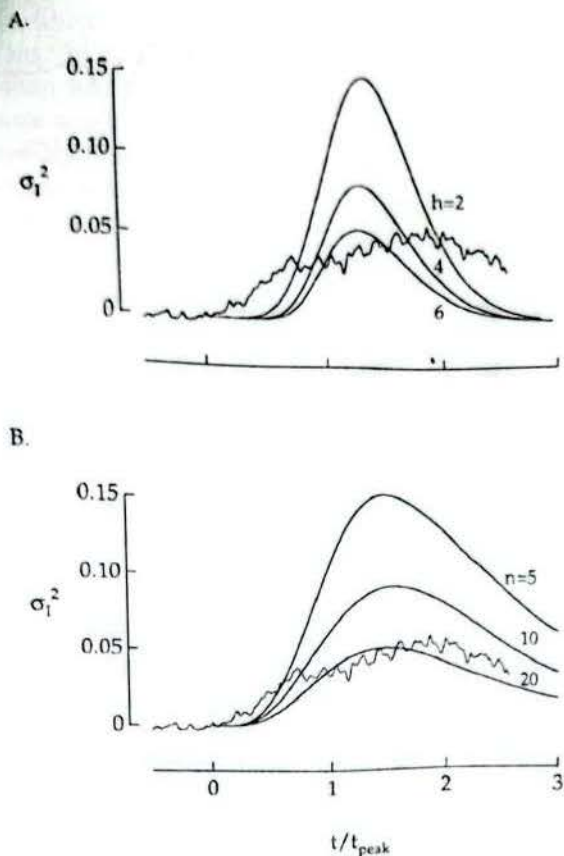


**FIGURE 18** Constraints on models for reproducibility from variance of single photon response. (A) Feedback. Suppression of fluctuations in the elementary response by feedback control of rhodopsin shutoff depends on the cooperativity with which the feedback acts; feedback signals acting with high cooperativities cause rhodopsin to shut off abruptly and thus more effectively decrease response fluctuations. The cooperativity required to explain the measured reproducibility was explored by calculating the time-dependent variance of the elementary response for a stochastic model in which rhodopsin shutoff was controlled by a feedback signal  $x$  accumulating linearly with time and acting with a cooperativity  $h$ . Thus the rate of rhodopsin shutoff was  $\alpha \propto x^h$ . The variance is shown for  $h = 2, 4$ , and 6. The noisy trace is the measured time-dependent variance of the elementary response from Fig. 5. A cooperativity of 4–6 was required to explain the measured reproducibility. (B) Multistep shutoff. Rhodopsin shutoff through multiple stochastic transitions could reduce variability in the elementary response. The number of steps required was explored by calculating the time-dependent variance for a stochastic model in which rhodopsin's activity decays through  $n$  first-order transitions. The traces plotted are for  $n = 5, 10$ , and 20. Fifteen to twenty transitions were required to explain the measured reproducibility.

more effective in reducing the variance, although the abrupt shutoff of rhodopsin's activity produced by this model confined the variance to a much shorter time window than the measured variance. Reduction of the variance to measured levels required a cooperativity greater than 4.

The main argument against this mechanism is that there are no obvious candidates for the feedback signal. The experiments in Results indicate that the signal cannot be  $\text{Ca}^{2+}$ , nor can it originate at or downstream of active transducin. Furthermore, the experiment of Figs. 14 and 15 suggests that the molecular events controlling most of rhodopsin's cumulative activity are independent of transducin

binding to rhodopsin, making rhodopsin kinase and arrestin unlikely feedback signals. Activated rhodopsin is not known to interact with any other molecular species.

#### Multistep shutoff of rhodopsin's catalytic activity

We believe that reduction in the intertrial variability of rhodopsin's catalytic activity by shutoff through a series of steps is the most likely explanation for reproducibility. Two experimental observations support this notion. First, rhodopsin's catalytic lifetime, at least at constant  $\text{Ca}^{2+}$ , was not explained by the time required for phosphorylation or arrestin binding (Figs. 7 and 15); thus other processes must contribute to rhodopsin deactivation. Second, the variability of the elementary response increased when phosphorylation was slowed, so that rhodopsin deactivation proceeded effectively as a single step, and this increase in variability was consistent with expectations if the current was fully sensitive to fluctuations in rhodopsin's activity (Fig. 17). Thus reproducibility failed when rhodopsin shut off effectively as a single-step process.

How many steps are required if reproducibility arises from multistep shutoff of rhodopsin's activity? To investigate this we calculated the time-dependent variance for the model described in Eqs. 7 and 10 and a stochastic model in which rhodopsin's activity decayed through a series of transitions. The rate constants of the transitions and activities of the preceding states were constrained so that on average rhodopsin's activity declined exponentially with a 2.5 s time constant. Fig. 18 B shows calculations of the time-dependent variance for rhodopsin shutoff through a series of 5, 10, and 20 transitions. Variability in rhodopsin's cumulative activity and in the elementary response decreased as the number of steps was increased. Reducing the variance of the elementary response to the measured level required 10–20 steps.

For multiple steps in rhodopsin shutoff to be effective, the transitions between states should be essentially irreversible. The large free energy difference ( $\sim 32$  kcal/mol) between isomerized, unphosphorylated rhodopsin and the rhodopsin-arrestin complex makes this energetically feasible. If this energy were divided equally among 15 steps, the ratio of forward to backward rate constants for each transition could be 20.

What molecular events might explain 10–20 steps in rhodopsin shutoff? Individual steps could be mediated by interactions of rhodopsin with other molecular species. For example, rhodopsin kinase might initially phosphorylate one of the four sites on the C-terminus, but the kinase might have to rebind to rhodopsin and move the phosphate several times before it reached a site permitting strong arrestin binding. Alternatively, individual steps might represent transitions intrinsic to the rhodopsin molecule. Multiple intrinsic states have been well documented by kinetic studies on ion channels, where the states are thought to represent distinct conformations of the channel protein. In a voltage-gated  $\text{K}^+$  channel, for example, there are over 15 distinct